UNIVERSITY OF COPENHAGEN

MASTER THESIS

The effect on Agulhas Rings by the Southern Ocean wind stress

Author:
Peder HEISELBERG

Supervisor:
Markus JOCHUM

A thesis submitted in fulfillment of the requirements
for the degree of Master of Science

Department of Climate and Geophysics
Niels Bohr Institute
University of Copenhagen

September 4, 2017

Declaration of Authorship

I, Peder HEISELBERG, declare that this thesis titled, "The effect on Agulhas Rings by the Southern Ocean wind stress" and the work presented in it are my own. I confirm that:

- This work was done wholly or mainly while in candidature for a research degree at this University.
- Where any part of this thesis has previously been submitted for a degree or any other qualification at this University or any other institution, this has been clearly stated.
- Where I have consulted the published work of others, this is always clearly attributed.
- Where I have quoted from the work of others, the source is always given. With the exception of such quotations, this thesis is entirely my own work.
- I have acknowledged all main sources of help.
- Where the thesis is based on work done by myself jointly with others, I have made clear exactly what was done by others and what I have contributed myself.

Signed:

Date:

"It is amazing that such clean plates can emerge from such dirty dishwater!"

Niels Bohr (dishwashing) to Werner von Heisenberg (wiping) after long reflection

University of Copenhagen

Abstract

Niels Bohr Institute
Department of Climate and Geophysics

Master of Science

The effect on Agulhas Rings by the Southern Ocean wind stress

by Peder HEISELBERG

High resolution $1/10^{\circ}$ General Circulationn Model (GCM) simulation data is analyzed to investigate the effects on Agulhas leakage via Agulhas Rings by change in Southern Ocean wind stress. 11 years of control data and 16 years of data with a 15% increase in Southern Ocean wind stress (tau15) is used. By developing a taylored search and track algorithm, 45 and 73 Agulhas Rings were detected in their respective dataset. A 12% increase in Agulhas Ring generation is found indicating a correlation but this is within one standard deviation of statistical fluctuations. A seasonal cycle in Agulhas Ring formation is visible in the tau15 data. The Agulhas Rings were found to have a mean radius of $140km$ and a translational velocity of $6cm/s$. A 14.5% increase in velocity were found in the tau15 data. The potential vorticity of the Agulhas Rings were found to be constant in the first $1000km$ of the Agulhas Current retroflection. Four years of low Agulhas Ring generation is observed to coincide with a lack of Natal Pulses in the Agulhas Current strongly indicating a relation. The excess production of Agulhas Rings by Natal Pulses is, however, within statistical fluctuations.

Acknowledgements

Thanks to my parents, family and friends. Special thanks Team Ocean for the ocean, programming and colormap related discussions and to my supervisor Markus Jochum who made this journey an absolute pleasure…

Contents

List of Figures

List of Tables

List of Abbreviations

AMOC	**A**tlantic **M**eridional **O**verturning **C**irculation
CESM4	**C**ummunity **E**arth **S**ystem **M**odel version **4**
GCM	**G**eneral **C**irculation **M**odel
MOC	**M**eridional **O**verturning **C**irculation
OGCM	**Ocean G**eneral **C**irculation **M**odel
POP2	**P**arallel **O**cean **P**rogram **2**
SSH	**S**ea **S**urface **H**eight
SLA	**S**ea **L**evel **A**nomaly
SIFT	**S**cale **I**nvariant **F**eature **Transform**
tau15	**15%** increase Southern Ocean wind stress

Dedicated to my family…

Chapter 1

Introduction

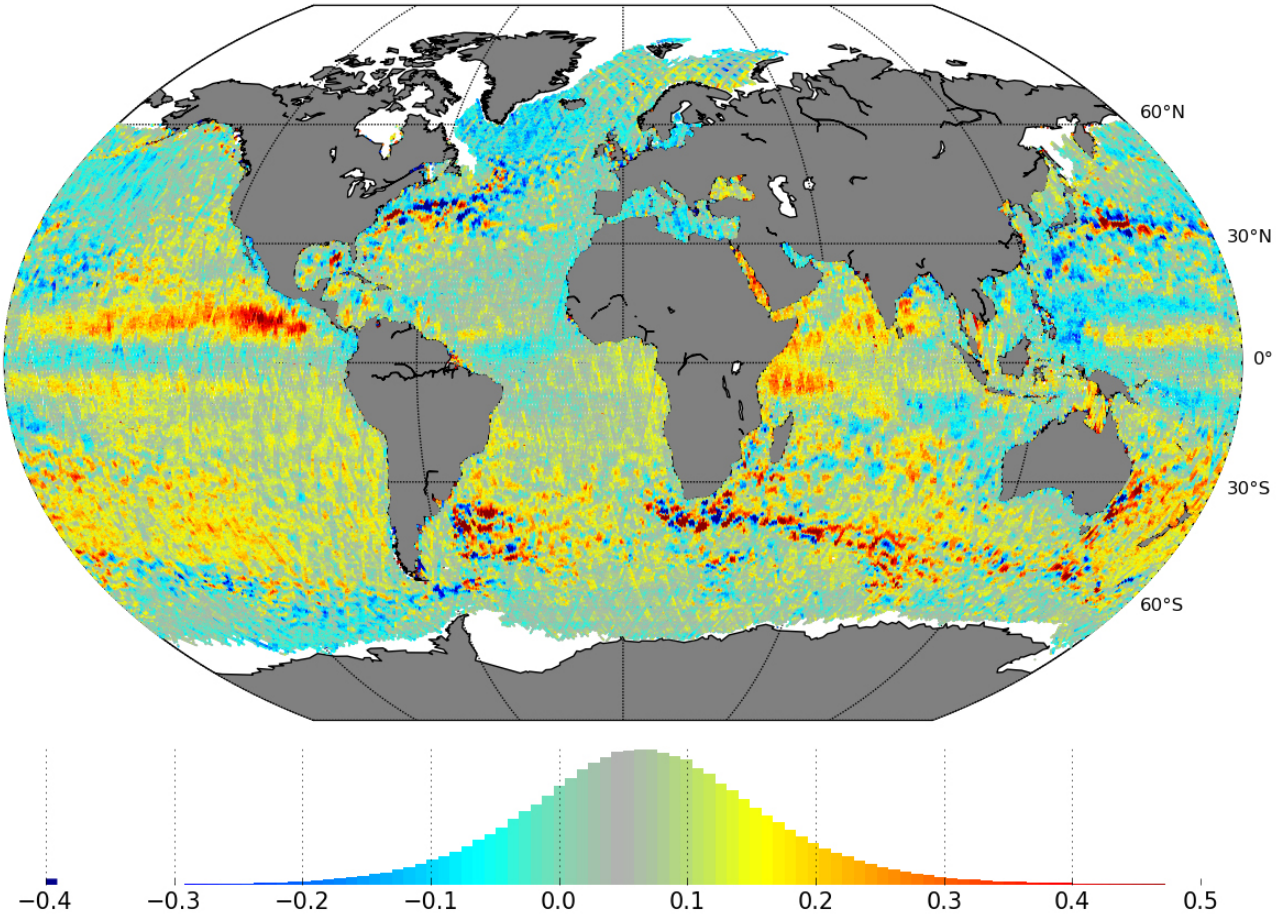

FIGURE 1.1: Sentinel-3A satellite earth observation altimetry data from 2016. Colorbar is in meters. A strong eddy field is visible in the Agulhas Current south of Africa. Also note the stripes in the data which are artifacts from the satellite trajectories. Image attained from http://www.esa.int/spaceinimages/Images/2016/05/Sea-level_variations_from_Sentinel-3A

1.1 The Agulhas Current

The Indian Ocean basin has a subtropical ocean gyre like many other ocean. This gyre circulate the water within the ocean from south to north. The ocean flow is directly driven by the wind stress curl in a relation known as the Sverdrup balance. In the western part of the gyre the African continent forms a wall at which the water flows south and recirculates back into southern part of the ocean forming a complete ocean gyre. This western part makes up a narrow band of the ocean and therefore gives rise to strong ocean currents. These currents are known as western boundary currents because of their position at the western boundary of the ocean gyres[1].

The Agulhas Current is the western boundary current of the Indian Ocean. It recirculates the warm salty water of the Indian Ocean. Some of this water does however leak into the Atlantic Ocean by shedding Agulhas Rings which as opposed to the Indian Ocean has a Meridional Overturning Circulation (MOC) that can exchange water between the Atlantic subtropical gyres on each side of the hemissphere and thereby the poles.

The upper part of the Agulhas Current is made up of the Mozambique Current and East Madagascar Current. Madagascar works as a shield for the Mozambique straight known for its modern day pirates. Mozambique eddies enter this straight from the north and exits to the south. The East Madagascar Current flows south along Madagascars coast and joins up with the current at the southern tip emitting large scale westward traversing Madagascar eddies.

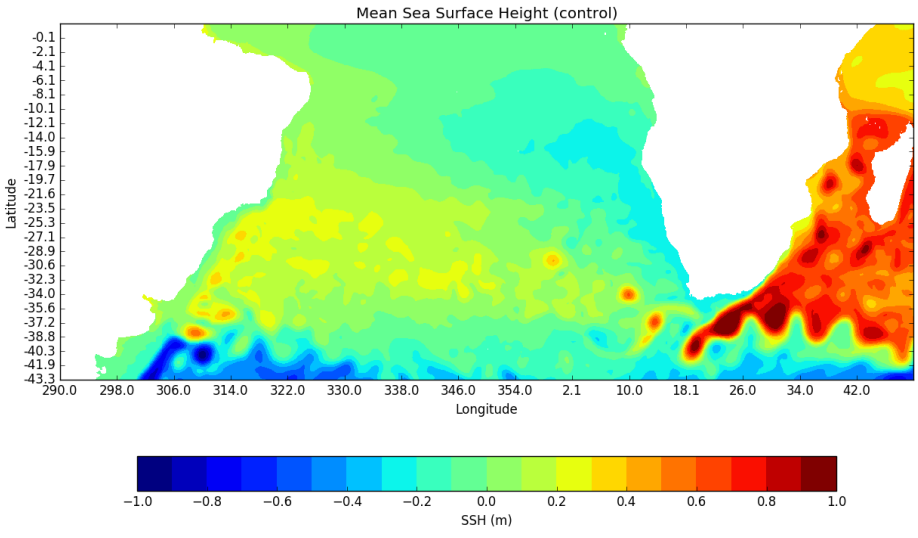

FIGURE 1.2: Snapshot of one month of monthly meaned SSH control data with three clearly visible Agulhas Rings west and southwest of South Africas.

[1]Gyres have opposite direction of flow northern hemisphere because the coriolis force changes sign.

As the current flows south along the African east coast where the continent ends before it would naturally return into the Indian Ocean. As it protrudes southwestward along Africas southern continental shelf it retroflects reversing direction and flows back into the Indian Ocean via the Agulhas Return Current.

The part of the current where it retroflects is known as the Agulhas Current retroflection. Here the current is very unstable and gives rise to Agulhas leakage primarily in the form of huge eddies known as Agulhas Rings that enter the Atlantic Ocean. It is one of the few places oceans exchange water this directly. The Indian Ocean waters are significantly warmer and saltier than that of the Atlantic which is a large factor for the Atlantic Meridional Ocean Circulation (AMOC). The AMOC allows the poles and oceans to connect. Thus changes to the AMOC are detrimental to the global climate. Agulhas Rings are therefore an essential component in understanding not only the current global climate but also that of the past and future.

These many aspects of the Agulhas Current makes it one of the most dynamically interesting boundary currents in the world.

1.2 Model and data

The numerical data used in this thesis stems from the Ocean General Circulation Model (OGCM) of the Community Earth System Model version 4 (CESM4), Parallel Ocean Program (POP2). POP2 is a validated global high resolution $1/10^{\circ}$[2] model [Small et al., 2014]. Using simulated data allows for numerical experiments to be conducted with variable control as opposed to using remote sensing satellite data. As seen in Figure 1.1 the satellite altimeter data contains satellite track artifacts seen as stripes in the image which must be corrected for.

A control run and a perturbation run with 15 percent increased wind stress on the southern ocean is analysed. Wind stress is commonly denoted with the greek letter τ. The runs will hensforth be respectively refered to as control and tau15. 11 years of control data and 16 years of perturbation data is analysed. The time series are possibly the longest in any study conducted on Agulhas Rings.

The data analysed is in the form of monthly mean sea surface height (SSH). Thus yielding 132 monthly meaned sets of control data and 192 sets of perturbation data.

It has previously been found that Southern Ocean winds have little effect on the strength of the AMOC [Jochum and Eden, 2015]. This thesis seeks to investigate change inter-ocean transport via Agulhas Rings caused by an increase in Southern Ocean wind stress.

First a comparison between the Agulhas Rings of POP2 and real life observations is made. Secondly Agulhas Rings of the control run are compared to the rings of the perturbation run. Lastly a supposed trigger mechanism for Agulhas Ring shedding is put under scrutiny.

[2] This translates to a $10km$ grid-spacing.

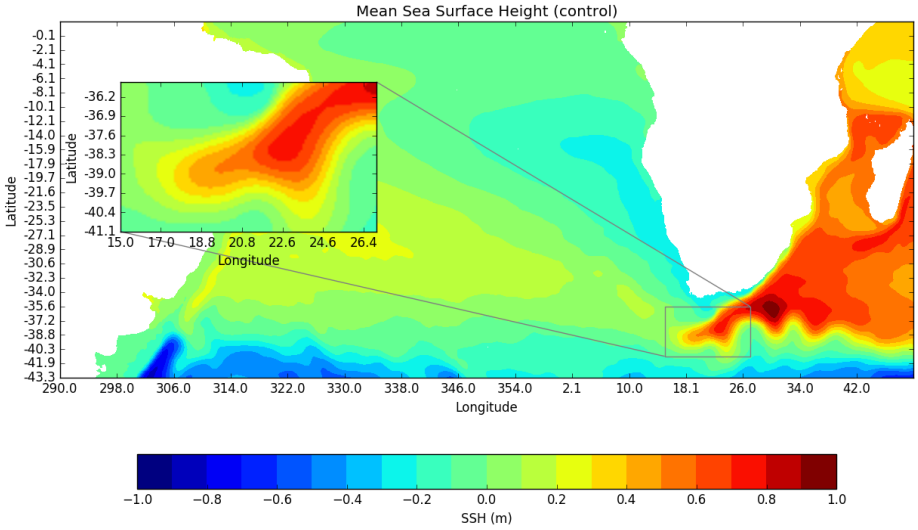

FIGURE 1.3: The mean sea surface height of the 132 months control data

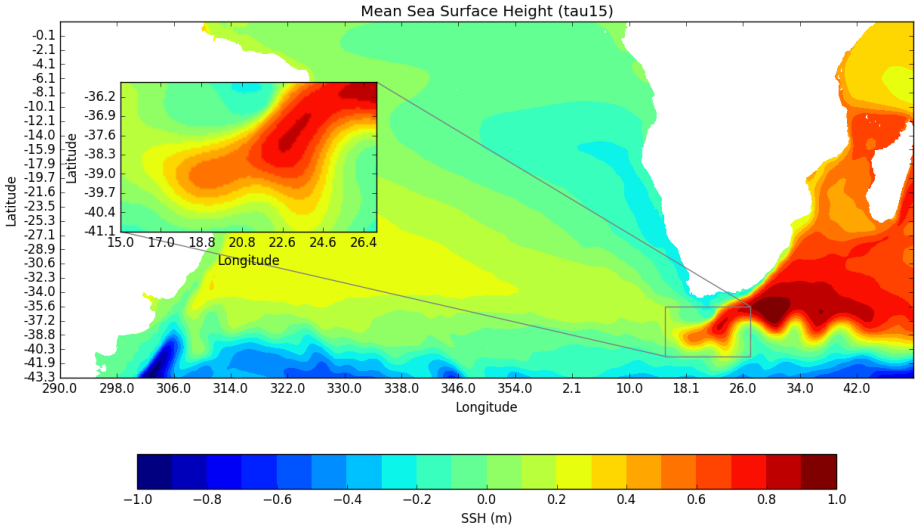

FIGURE 1.4: The mean sea surface height of the 192 months tau15 data

1.3 Control and tau15 data

At first glance a few noticeable differences immediately becomes apparent. The increased mean SSH of the atlantic subtropical gyre between Figure 1.3 and Figure 1.4 which could be attributed to an increase in steady background flow supported by the lack of increase in variance of Figure 1.6. One could this assume the same is the case for the Agulhas Current.

The return current is far more contained within a narrow high variance jet in the tau15 data compared to the more smeared jet of the control data.

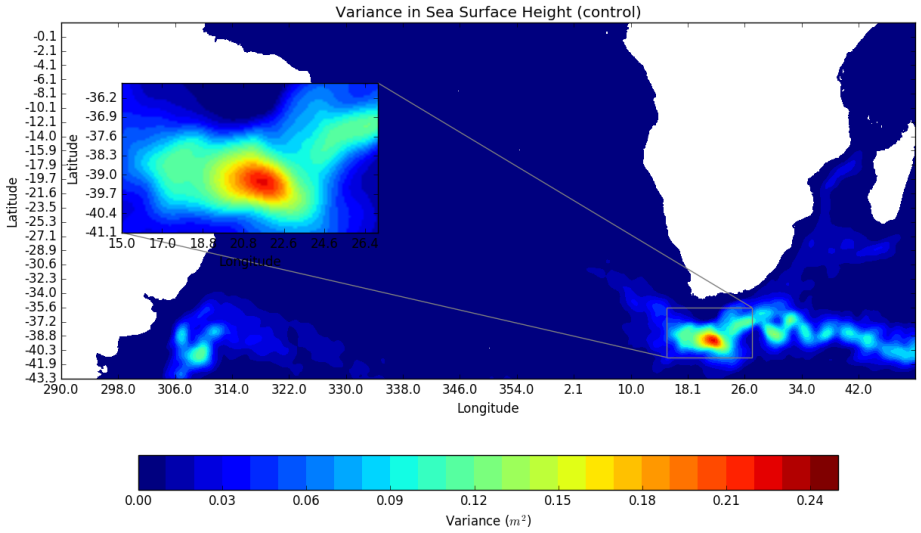

FIGURE 1.5: The temporal variance in sea surface height of the control data.

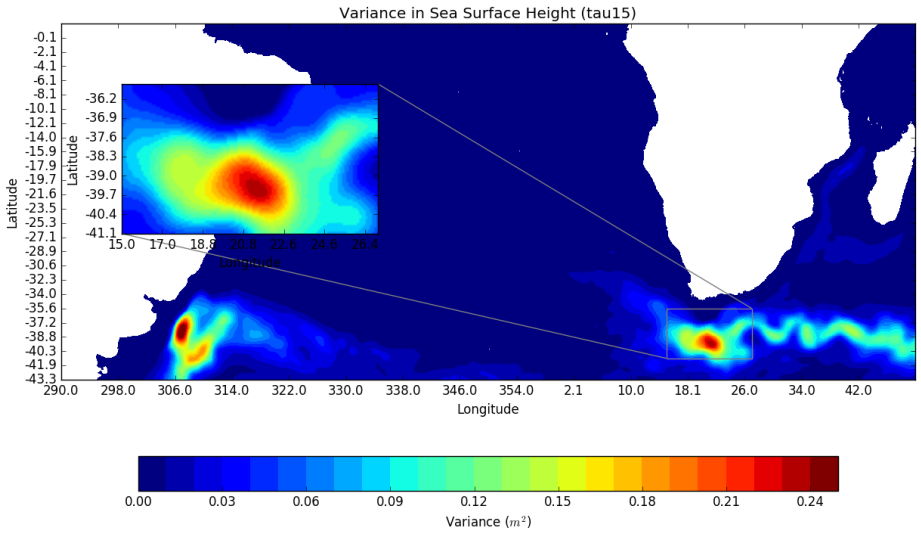

FIGURE 1.6: The temporal variance in sea surface height of the tau15 data.

1.3.1 The Agulhas Current Retroflection

The Agulhas Retroflections naturally extends and shortens with a mean position between 16° to 20°east longitude[Lutjeharms and Ballegooyen, 1988]. Due to the instability of the retroflection as it extends westward the loop closes in on itself effectively shortening the current potrusion and emitting Agulhas leakage. This region would have a significantly high variance which is at $21.5°$ east in both Figure 1.5 and Figure 1.6. The mean position of the retroflection is also in good accordance with previoulsy stated observations in Figure 1.3 and Figure 1.4 with a diameter of about $300km$.

1.3.2 The Mozambique Current and the East Madagascar Current

Both Mozambique eddies and Madagascar eddies can be seen in Figure 1.2.

There is a significant variance decreases in the Mozambique straight, just south of Madagascar and their connection to the retroflection in Figure 1.7 and Figure 1.8. Upstream effects like Mozambique and Madagascar eddies could thus have less impact on the downstream current in the tau15 data.

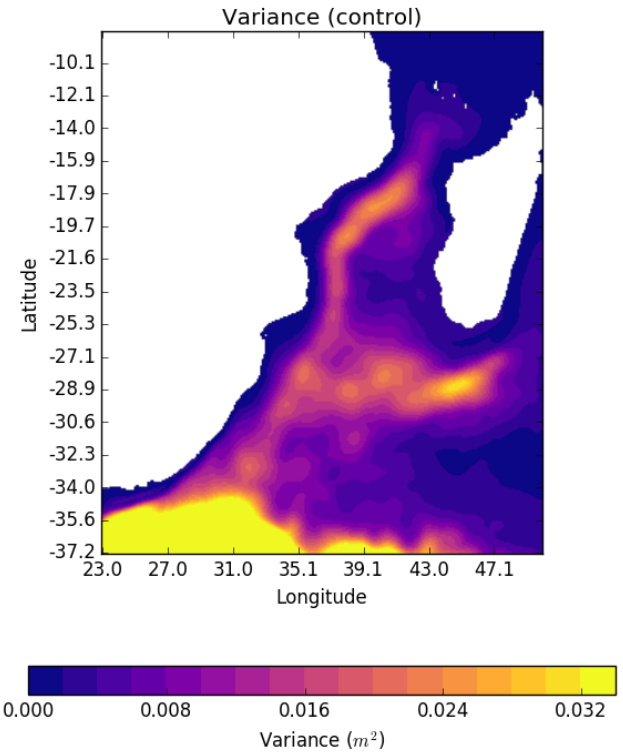

FIGURE 1.7: Temporal variance of the upper Agulhas Current in control data

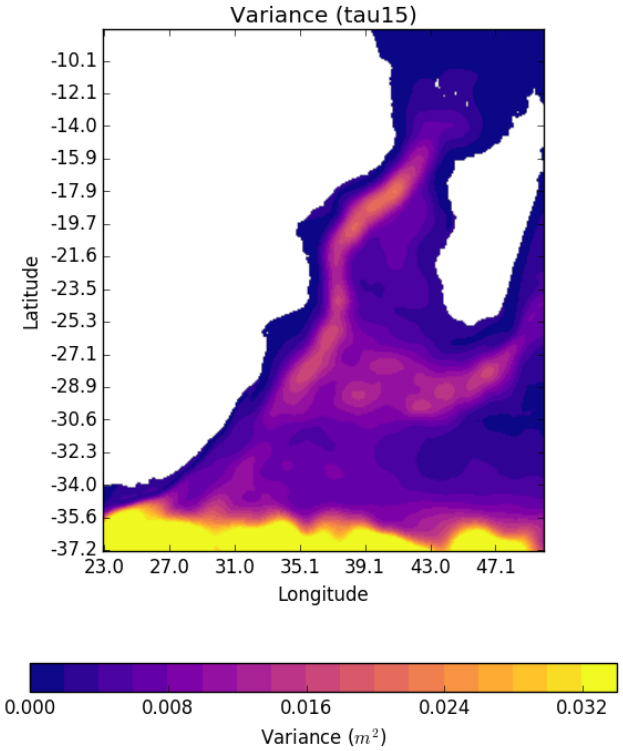

FIGURE 1.8: Temporal variance of the upper Agulhas Current in tau15 data

Chapter 2

Agulhas Rings

Agulhas Rings have been thorougly studied by oceanographers as they facilitate inter-ocean transport of warm salty Indian Ocean waters into the Atlantic. This transport of water clearly depends on the frequency of which Agulhas Rings Current shed the Agulhas Rings. Observations of poleward movement of the Southern Hemisphere westerlies in the last three decades has been linked to an increase in Agulhas leakage owing to a weaker Agulhas Current [Sebille et al., 2009]. An increase in inter-hemispheric salt transport originating from Agulhas leakage via the North Brazil Current by 25 percent was also found [Biastoch et al., 2009]. It is currently believed that Agulhas leakage through Agulhas Rings form the upper layer of the Atlantic overturning circulation[Souza et al., 2011].

It has been proposed that Agulhas Ring formation happens in order to balance the momentum flux of the current as it retroflects by generating westward moving rings that exert an eastward force, like the recoil of a classic naval cannon[Pichevin, Nof, and Lutjeharms, 1998]. Agulhas Ring formation can however also happen via ring-merging events in the Cape Basin as opposed to a pinch off from the Agulhas Current Retroflection [Wang, Beron-Vera, and Olascoaga, 2016].

From satellite mesurements Agulhas Ring velocity of 3-9 cm/s and diameter of 150-300 km have been found [Gordon and Haxby, 1990][Byrne, Gordon, and Haxby, 1994][Olson and Evans, 1985][Lutjeharms and Ballegooyen, 1988].

The first internal Rossby radii of deformation is $25km - 40km$ in the Agulhas region[Houry et al., 1987], Agulhas Rings are therefore not a product of conventional nonlinearity.

2.1 Finding Agulhas Rings

An Agulhas Ring is easy to spot as it is at almost all times a large SSH anomaly in the subtropical gyre along with its characteristic ring shape. The gyre however has a general nonzero SSH. Measuring the SSH of an Agulhas Ring would therefore also be a measure of the gyres mean height and any seasonal changes to that specific place. This is corrected by subtracting the mean SSH of the ocean gyre to remove the geospecific variations in gyre SSH. Next any seasonal variation is removed by finding the mean SSH of every individual month and then subtracting it from the

data, e.g. the mean SSH of every january is subtraced from every january. Left is a sea level anomaly (SLA) map with no seasons and a zero mean.

$$SLA = SSH - SSH_{mean} - SSH_{season} \tag{2.1}$$

The true SSH of the Agulhas Rings can be detected from the SLA map.

plot SLA map and compare to a previous SSH map

2.2 Anticyclonic eddies

Earths rotation cause coriolis forces on currents which again cause a pressure difference that raises or depresses the SSH. The balance between the two is called the geostrophic balance. Simple approximations lets us calculate this balance between the pressure (P) gradient and the coriolis force.

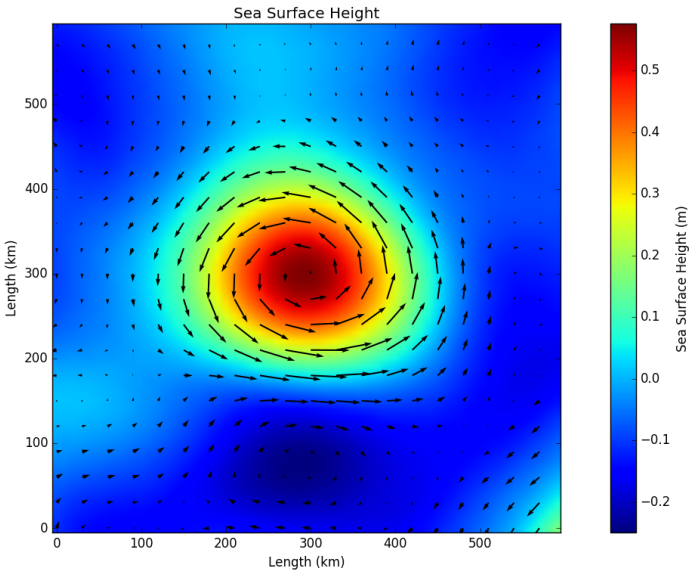

FIGURE 2.1: SSH of a typical Agulhas Ring with geostrophic velocity arrows as given by Eq. 2.4 and Eq.2.5

.

The horizontal components in the geostrophic balance is

$$\rho f \vec{v} = -\frac{\partial P}{\partial y} \tag{2.2}$$

$$\rho f \vec{u} = \frac{\partial P}{\partial x} \tag{2.3}$$

where ρ is the density of water, $f = 2\Omega \sin(\theta \frac{2\pi}{360})$, the coriolis parameter with angular velocity of earth $\Omega = 7.3 \cdot 10^{-5} s^{-1}$, and θ is the latitude[Pedlosky, 1996].

Inserting $P = \rho g\big(h(x,y) + H\big)$ under assumption of a homogenous ocean of constant density in hydrostatic balance with a constant water column height H that has a zonal and meridional variable height h.

This leads to the geostrophic velocities

$$u = -\frac{g}{f}\frac{\partial h(x,y)}{\partial y} \tag{2.4}$$

in the zonal direction, and

$$v = \frac{g}{f}\frac{\partial h(x,y)}{\partial x} \tag{2.5}$$

in the meridional direction

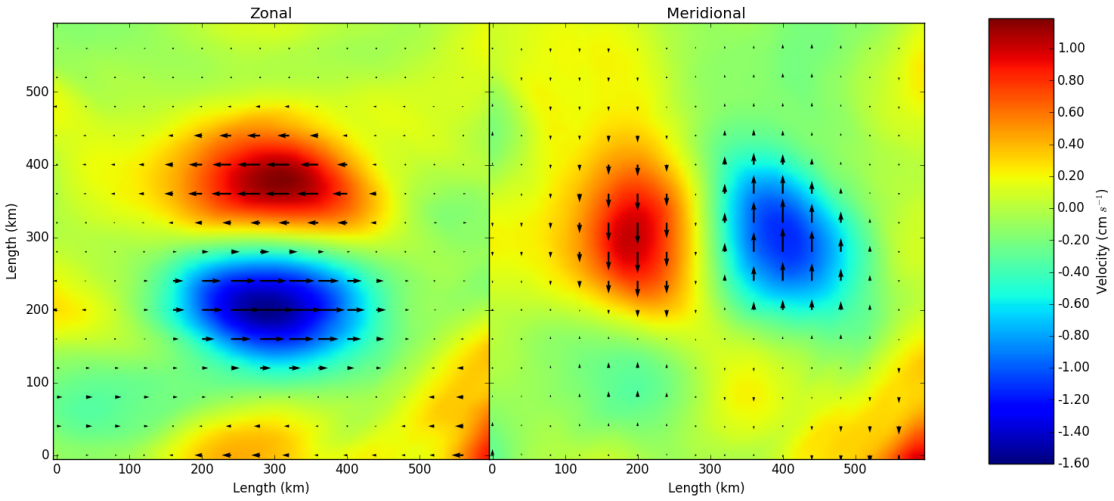

FIGURE 2.2: Geostrophic velocity of a typical Agulhas Ring. Arrows show direction of the velocity.

The *relative* vorticity of an object describes the local spinning motion in a continuum *relative* to a plane of reference. It depends on hemisphere because the coriolis parameter changes sign once you cross the equator. The relative vorticity of an eddy is the curvature of it and can therefore also be considered a proxy for the strength of an eddy.

The geostrophic relative vorticity is given by

$$\zeta = -\frac{\partial u(x,y)}{\partial y} + \frac{\partial v(x,y)}{\partial x} \simeq \frac{g}{f}\nabla^2 h(x,y) \tag{2.6}$$

This would be equal to the laplacian of the SSH map, if the coriolis parameter were not dependent of the meridional gradient.

In our case a large Agulhas Ring with a positive SSH would have a negative relative vorticity and therefore an anti-cyclonic spin.

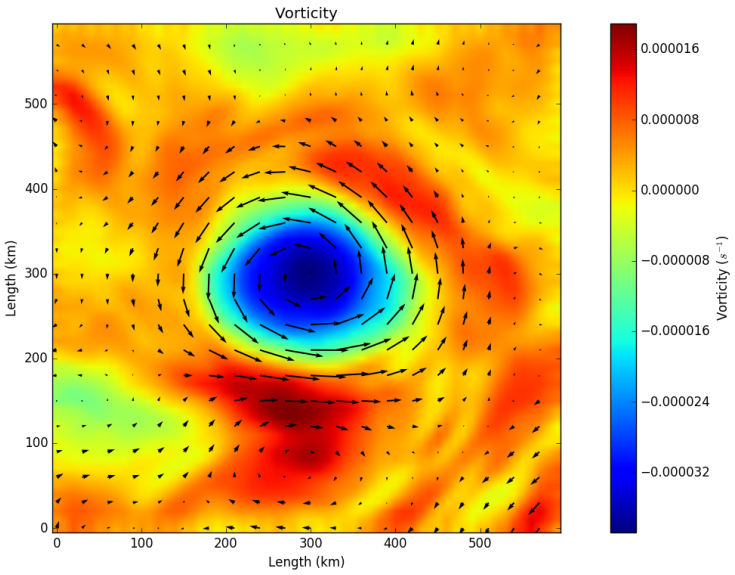

FIGURE 2.3: Relative Vorticity of a typical Agulhas Ring. Arrows show geostrophic velocities.

The ring center is at the minimum of its vorticity with sea surface height given by the SLA map. The radius of a ring is the distance from the center to the zero vorticity mark (i.e where it stops spinning).

The potential vorticity on the other hand is a measure of proportionality between the relative vorticity and the planetary vorticity. It can only be changed by frictional forces or non-abaticly thus it is considered a conserved quantitiy.

$$q = \frac{\zeta + f}{H} \tag{2.7}$$

with H being the water column height mentioned above.

How are the Agulhas Rings located[1]. Agulhas Rings are not the only anti-cyclonic structures in the ocean. Thus simply searching for local relative vorticity minima is bound to turn up the heaps of unwanted structures that also populate the ocean (See black dots in Figure 2.4). The trick to counteract this is to create a band pass filter using the difference between two gaussianly smoothed SSH maps (See green dots in Figure 2.4). The difference of gaussians (DoG) is a good approximation to the laplacian operator and allows sampling within a scale space(band).

The DoG method does however introduce a small uncertainty due to its approximative nature but at the same time acts similar to thresholding structures with regards to size and SSH profile at the same time.

[1]The thousand lines of code used to make the complete algorithm laid out in this chapter can be optained from the author on request.

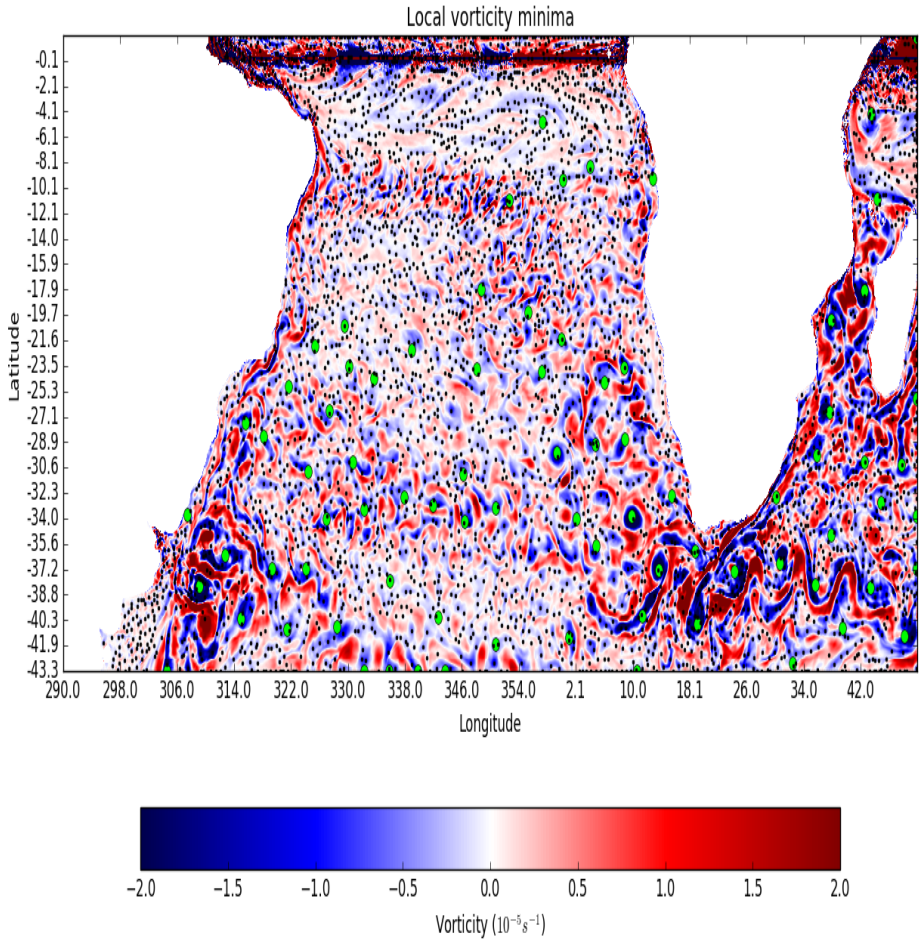

FIGURE 2.4: Relative vorticity of the data shown in Figure 1.2. Black dots denotes local minima found in the relative vorticity while green dots are local minima found in DoG

2.3 Tracking Agulhas Rings

Once an Agulhas Ring is out in the open ocean it behaves very simplistic. The trouble starts when attempting to identify large scale anti-cyclonic structures close to the retroflection. It is extremely difficult to determine which structures near the Cape of Good Hope is an Agulhas Ring in Figure 2.4. It quickly becomes guess work the closer you get to the retroflection.

As an Agulhas Rings exits the retroflection it is subject to stretching and squeezing in combination with an observed exponentially decreasing SSH signature with distance from the retroflection[Byrne, Gordon, and Haxby, 1994]. Until the ring has stabilized the large variance of SSH renders it out of the question as a stable ring parameter over time. The SSH signature is of course still a tell tell sign of Agulhas

Current origin.

One of the unique features of Agulhas Rings is their longevity. Regardless of the chaotic circumstances of ring inception it stays coherent. Agulhas Rings are large scale anti-cyclonic eddies with a minimum lifetime of several months. Some of the objects in Figure 2.4 might in fact be Agulhas Rings in infancy and following them in time will reveal this.

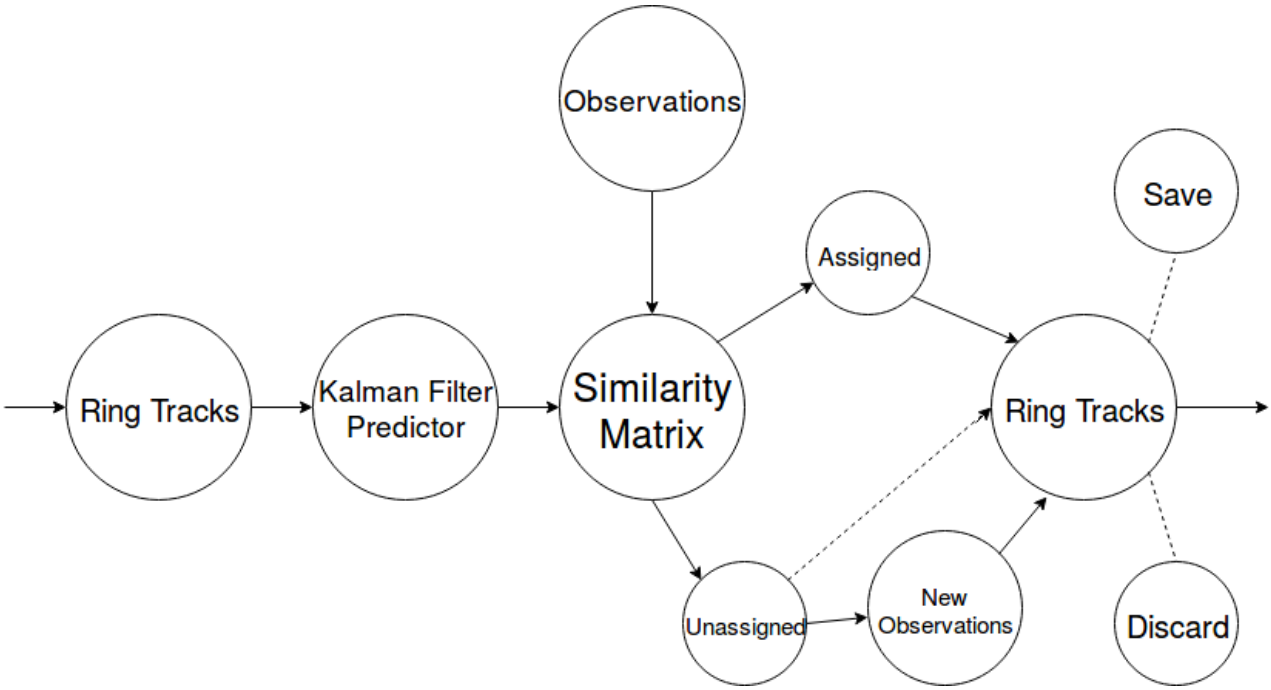

FIGURE 2.5: Flow chart showing the inner workings of the Agulhas Ring tracking algorithm. Detailed describtion in Section 2.3

The overall structure of the algorithm is shown by the flow chart of Figure 2.5. A more detailed description is as follows:

Ring Tracks Ring tracks contains all the information about a ring at any given time throughout its lifetime. Say a ring is found at time t with a lifetime of n months. The center of the ring is then given by the coordinates $X = x_0, x_1, \cdots, x_n$ and $Y = y_0, y_1, \cdots, y_n$. As well as the SSH, radius, vorticity, and time of detection.

Kalman Filter Predictor Given a series of previous coordinates of an Agulhas Ring ($X = x_0, x_1, \cdots, x_n$) the Kalman filter predicts the next position (x_{n+1}) based on all the previous positions and their associated errors. If a ring is observed near x_{n+1} the prediction is adjusted, if no observation was made the Kalman filter [2] prediction is used to predict the next position x_{n+2}.

[2]The Kalman filter has been implemented according to Kalnay, [2003].

Similarity Matrix The Kalman filter estimates are compared to observations. This is done by setting up the matrix

$$C^{i,j} = \sqrt{\left(x^i_{est} + x^j_{obs}\right)^2 + \left(y^i_{est} - y^j_{obs}\right)^2} \tag{2.8}$$

Where x^i_{est} and y^i_{est} is the estimated next position of the i'th Agulhas Ring tracks given by the Kalman filter and x^j_{obs} and y^j_{obs} is the observed anomalies.

Each index of the similarity matrix is the distance between the estimated next positions of rings at time $t = n \rightarrow t = n + 1$ and the observed position of rings at time $t = n+1$. The matrix is solved using a hungarian algorithm which optimally assigns the estimates to the observations in order to minimize the resulting assignment similarity (cost). Estimates and observations can only be assigned once.

Assigned/Unassigned Tracks Observations that are assigned an estimate are added to that specific track updating the rings position.

The dotted arrow in Figure 2.5 denotes an inbuilt buffer in the algorithm. If a ring track is unassigned which can happen for several reasons, most of whichs are mentioned at the top of this section, it is given a strike instead of being immediately deleted/saved. This is an inbuilt feature of the Kalman filter. It is therefore possible for example for two rings to collide into one ring and then divide into two rings again without stopping the tracking of any ring involved thereby also avoiding double counts.

New Observations Unassigned observations are either false positives or newly detected Agulhas Rings. In any case they are thresholded with regards to their SSH and position, since rings are spawned in the retroflection with a large SSH. Observations that fit the criteria are added to the list of ring tracks. At $t = 0$ there are no ring tracks. All observations are therefore treated as new observations.

Save/Discard Before the ring tracks are passed on to iterate through the algorithm again their propagation direction and the number of continues strikes in the track is checked. If the number of strikes exceeds a predetermined limit the ring track is either saved or discarded based on the length of rings lifetime.

2.4 Analysis of results

Agulhas Ring tracks found with the algorithm are shown in Figure 2.6 are analyzed. Below are a series of plots. Month since detection (upper part) is compared to the distance from the retroflection (lower part) as well as differences between control (blue) and tau15 (red) data sets. The distance to the retroflection is smoothed with

a $50km$ or 1° radius running mean to increase readability. Colored bands in corresponding colors of one sigma and the raw data is also shown. The retroflection position is set to 38.02°S and 20.05°E. A high similarity between the data in the first few months of the upper half of the graphs and initial values in the lower part indicates the effectiveness of the algorithm to detect Agulhas Rings close the retroflection.

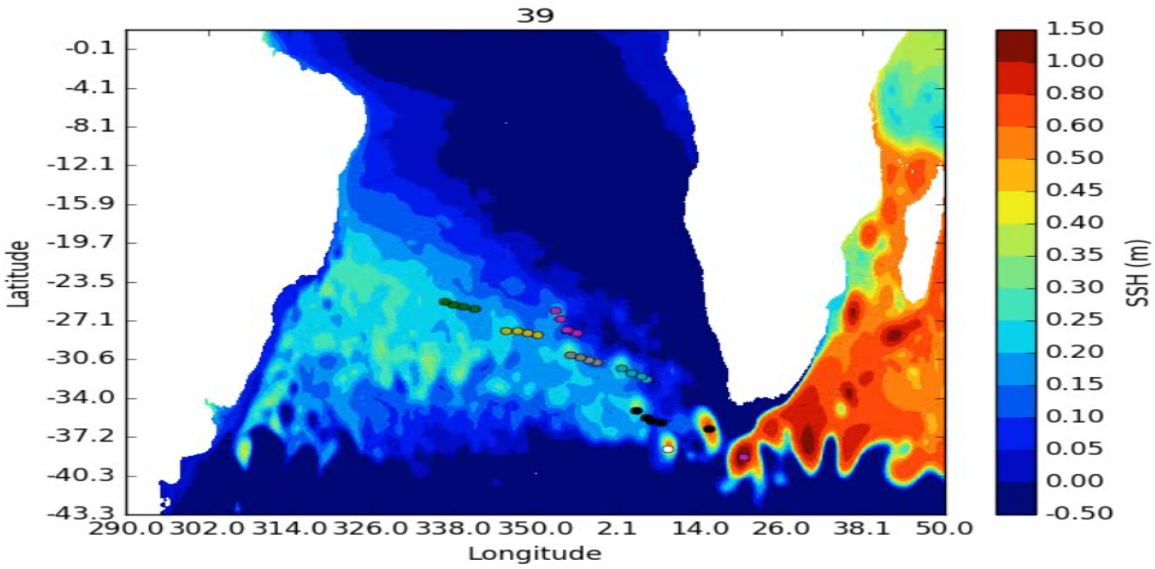

FIGURE 2.6: Trails of Agulhas Rings found with the algorithm. This figure is a shapshot from an animation showing Agulhas Rings traversing across the Atlantic Ocean created from the output of the algorithm described in Section 2.3. Dots denotes current position and up to three months prior positions. Figure title denotes the month in which the snapshot is taken.

2.4.1 Sea Surface Height

The sea surface height shown in Figure 2.7 is measured from the SLA map given by eq: 2.1. This leads to a lower height right at the retroflection. The unaltered SSH would be higher at this point and thus look more like an exponential decay but at later stages more effected by the Atlantic subtropical gyre seasonal behaviour. The figure is very similar to Figure 8(b) in Byrne, Gordon, and Haxby, [1994] which shows anomaly SSH of satellite observed decaying Agulhas eddies. No difference is found between control and tau15 data.

2.4.2 Velocity

Agulhas Rings propagate at a constant mean rate of $5.4 \pm 0.6 cm/s$ in the control data and $6.2 \pm 0.8 cm/s$ in tau15 data (shown in Figure 2.8. This is an increase of 14.5% which is suspiciously similar to the increase of 15% wind stress between the two datasets and indicates a relation.

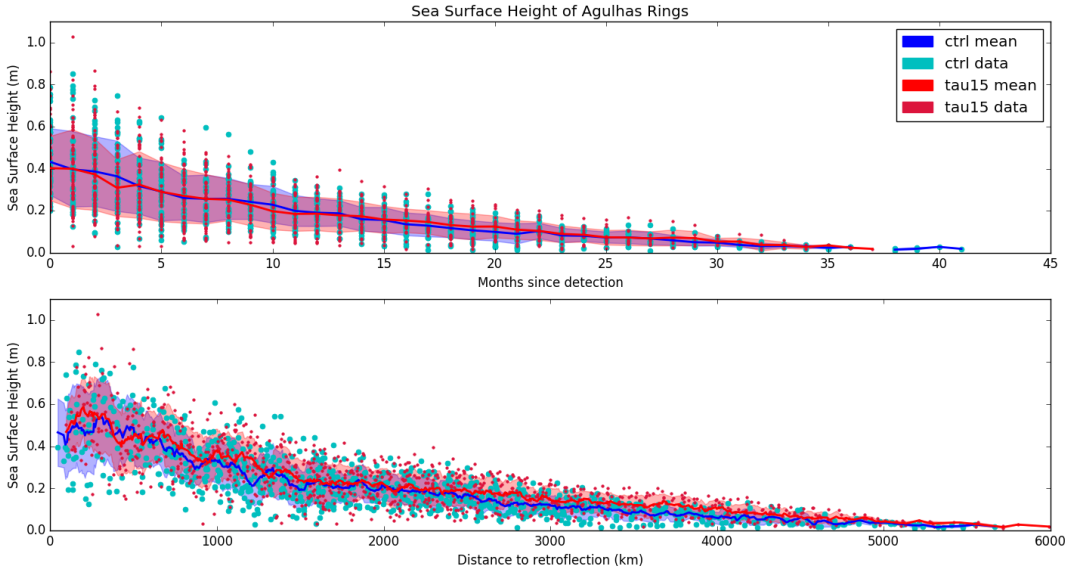

FIGURE 2.7: Sea surface height anomaly of Agulhas Rings from detection to demise found by the algorithm. Blue and red lines are the mean of respectively control and tau15 data. Bottom graph is a $50km$ running mean. Red and Blue bands are one sigma from their respective mean. Cyan and crimson dots are raw data.

The velocities has a larger variability in their early lifetime. The velocities found are in agreement with velocities the measured by satellite laid out in Section 2.

One might question the data points showing zero or close to zero velocity. This is mainly a feature of the Agulhas Rings that are shed in a southwestward direction as they come to a halt before changing direction northwestward.

Values above two sigma are due to *jumping* in the algorithm as it tracks the rings. This is similar to taking a wrong turn while following your car GPS, it keeps following your expected path for a while before jumping back to your actual position. The same can occur for the Agulhas Rings as they do not alway follow the predicted route.

2.4.3 Radius

The ring radius of the Agulhas Rings of Figure 2.9 which is in agreement with observations mentioned in Section 2. Mean radii of Figure 2.9 are $138.9 \pm 18.6km$ for control and 139.6 ± 10.3 for tau15. There is no change in radii of the Agulhas Rings between the data sets.

The radius seems to have a trend of decreasing after exiting the retroflection before slowly increasing again. This trend however happens within one sigma. As described in section 2.2 the ring radius is dependent on the relative vorticity potential. If this potential is skewed the radius will be off. A number of features can be responsible for this. Stretching and squeezing cause the rings to elongate, rings breaking up which is especially visible at the ladder parts of Figure 2.9, collisions

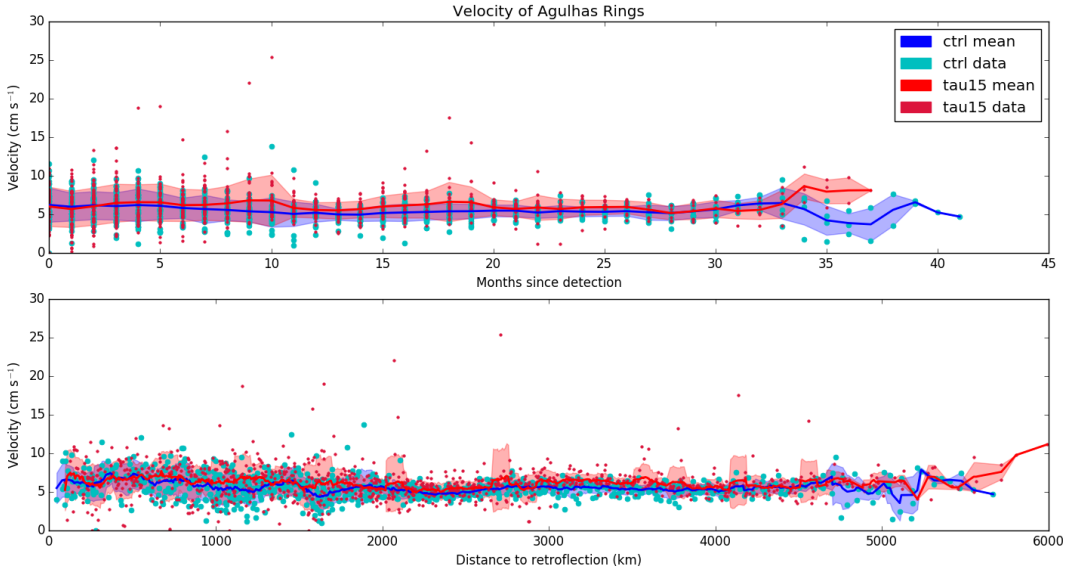

FIGURE 2.8: Translational velocity of Agulhas Rings (see Figure 2.7).

with other rings, and so on. The skewed potential can cause the measurement to overflow leading to an inflated radius.

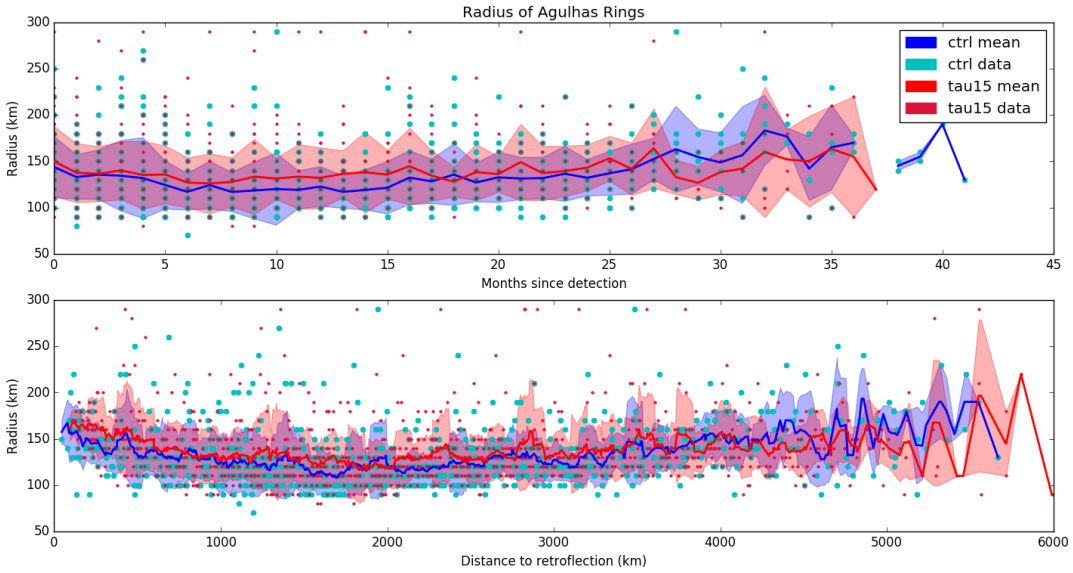

FIGURE 2.9: Radius of Agulhas Rings (see Figure 2.7).

2.4.4 Relative and Potential Vorticity

The relative vorticity as shown in Figure 2.10 decreases after the Agulhas Rings exit the retroflection but then slowly increases and approaches zero or a lower bound needed for ring coherence. Eventually the Agulhas Ring has to dissipate and flatten.

Therefore its curvature has to decrease to zero. From eq. 2.6 the curvature of the ring is proportional with the relative vorticity which thereby also has to decreases to zero. In turn this also means that the SSH has to decrease which can be seen in Figure 2.7.

It is clear from Figure 2.11 that the potential vorticity q given by eq: 2.7 of Agulhas Rings is not a conserved quantity.

However in the first $1000km$ it is constant. The northward movement of the rings cause an increase in planetary vorticity that has to be balanced by a decrease in relative vorticity. The Agulhas Rings has to increase their strength. One way to do this is by combining with smaller mesoscale eddies and filaments that inhabit the Cape Cauldron[Luthjharms and Cooper, 1996].

Another factor may be sea mounts. Conservation of potential vorticity (see eq. 2.7) states that a decrease in water column height leads to an increase in relative vorticity and thereby a weakening of the eddy. Agulhas Rings crossing large sea mountain ranges like the Walvis ridge which are approximately $1500km$ from the retroflection would thus coincidentally be visible in both the control and tau15 data. This is however not observed within the data fluctuations.

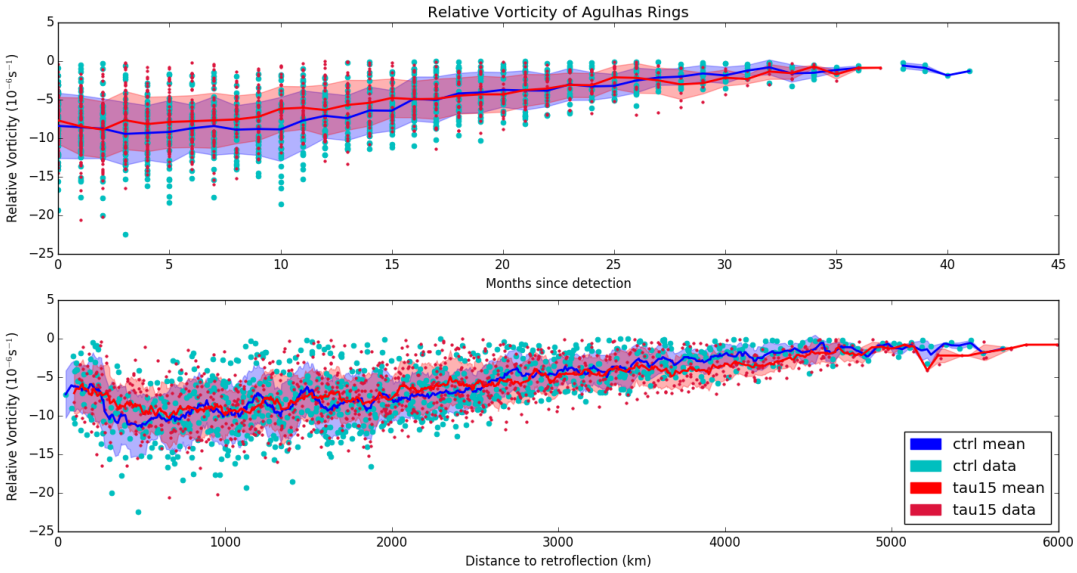

FIGURE 2.10: Relative vorticity ζ of Agulhas Rings (see Figure 2.7)

2.4.5 Rings

A total of 45 Agulhas Rings were detected in the control data and 73 in the tau15 data. The cumulative sum in Figure 2.12 indicates the ideal ring generation is the same. After the first 11 years where the control data ends the number of rings generated is almost identical. The nonzero starting value is due to already generated rings.

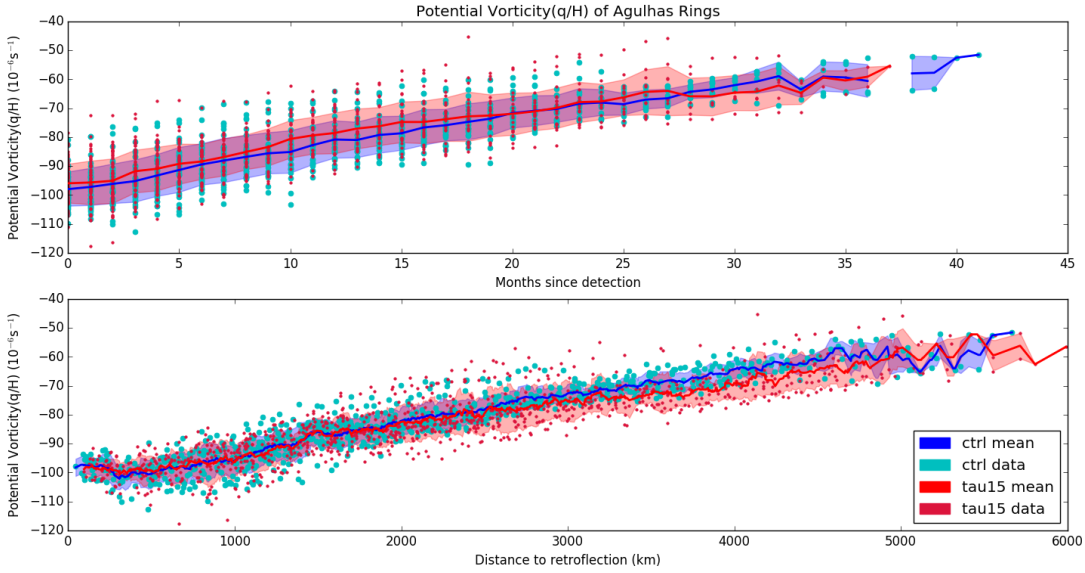

FIGURE 2.11: Potential vorticity q of Agulhas Rings (see Figure 2.7)

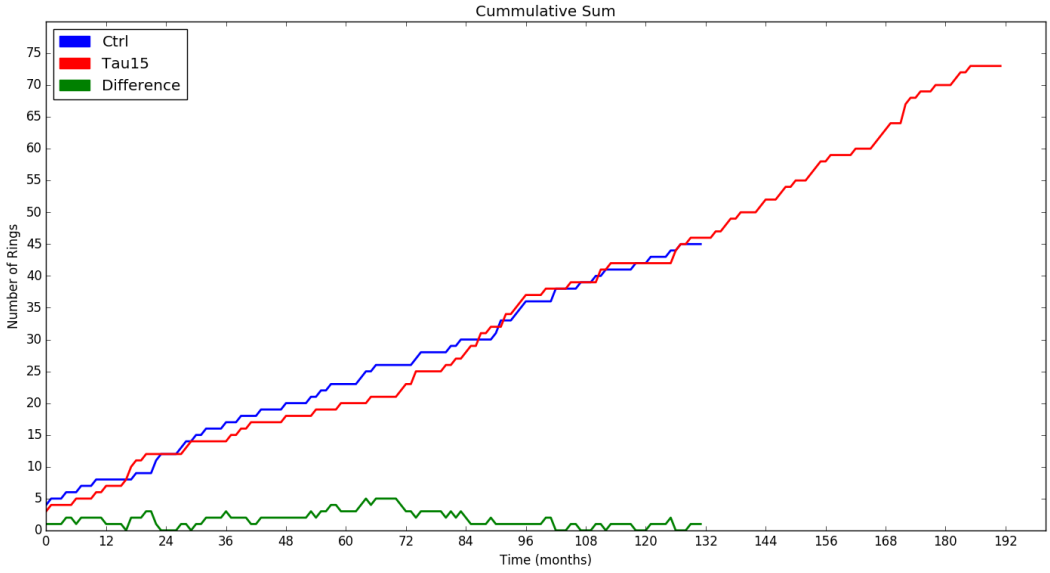

FIGURE 2.12: Cummulative sum of Agulhas Ring detection. (b) control, (r) tau15, (g) difference between control and tau15.

Figure 2.13 shows that ring shedding has favourable months. For example there are 11 months of september in the control data but only one ring is observed in this month it is however still within two sigma. This could be down to the inherit randomness of ring generation as there is no clear seasonal variation. The tau15 data on the other hand seems to have a seasonal signal[3] varying around the mean, building up at the southern hemispheres fall and spring and decrease at the end of

[3]The southern hemispheres seasons are opposite to the northerns

winter/summer. The increase in windstress could directly or indirectly induce this seasonality.

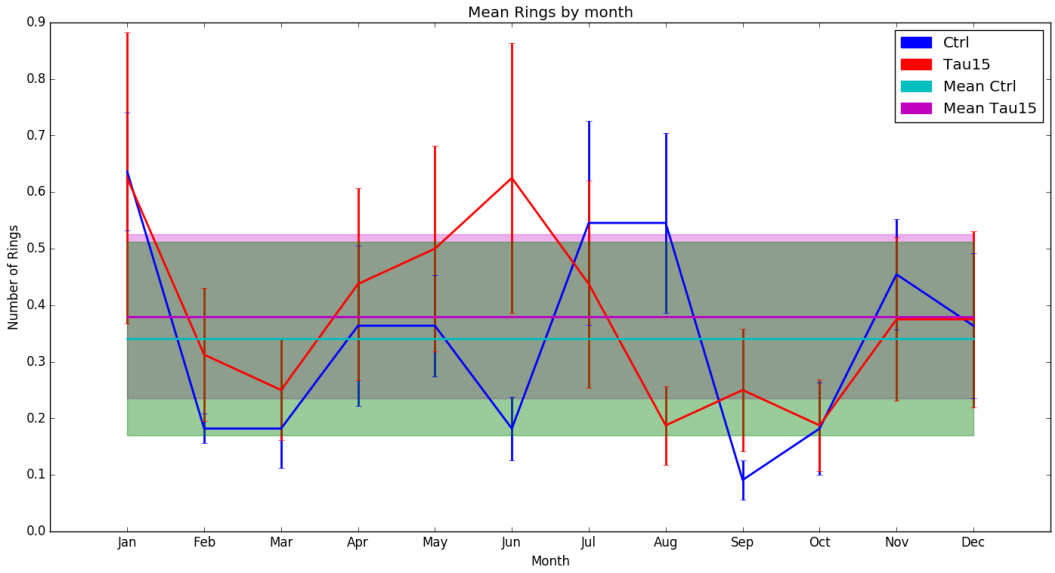

FIGURE 2.13: Agulhas Ring detections by month with standard deviation errorbars.(blue) control, (red) tau15, (cyan) mean of control with corresponding one sigma band, (purple) mean of tau15 with corresponding one sigma band.

Annual variation of ring generation is shown in Figure 2.14. A low variability of ± 1 rings after the first year dominates the control data which has a mean of 4.1 ± 1.4 rings per year compared to the slight increase in tau15 4.6 ± 2.1 rings per year. This is a change of 12% rings per year. However, tau15 has a comparatively higher inter annual variation with a low between year 2 and 7 which is also seen in Figure 2.14. Therefore the 12% increase in rings is within statistical fluctuations[4] within, and one cannot necessarily conclude that the increased wind stress is the cause.

2.5 Discussion and conclusion

The Agulhas Rings of POP2 are in good accordance with altimeter satellite observations. Differences in ring dynamics between control and tau15 data are neglicible except for the translational velocities. Wind stress has no say in the dimension or dynamics of Agulhas Rings. The 15% increase in wind stress directly correlates with the 14.5% increase in translational velocity of Agulhas Rings in the tau15 data.

Table 2.1 contains a list of observed Ring-shedding events by different authors. Combined, the observations estimate an annual generation of 6 ± 1.2 rings per year. The model underestimates the number of Agulhas Rings generated in the control

[4]The statistical fluctuations assuming random non-correlated generation in a number N, is $\sqrt{N}$.

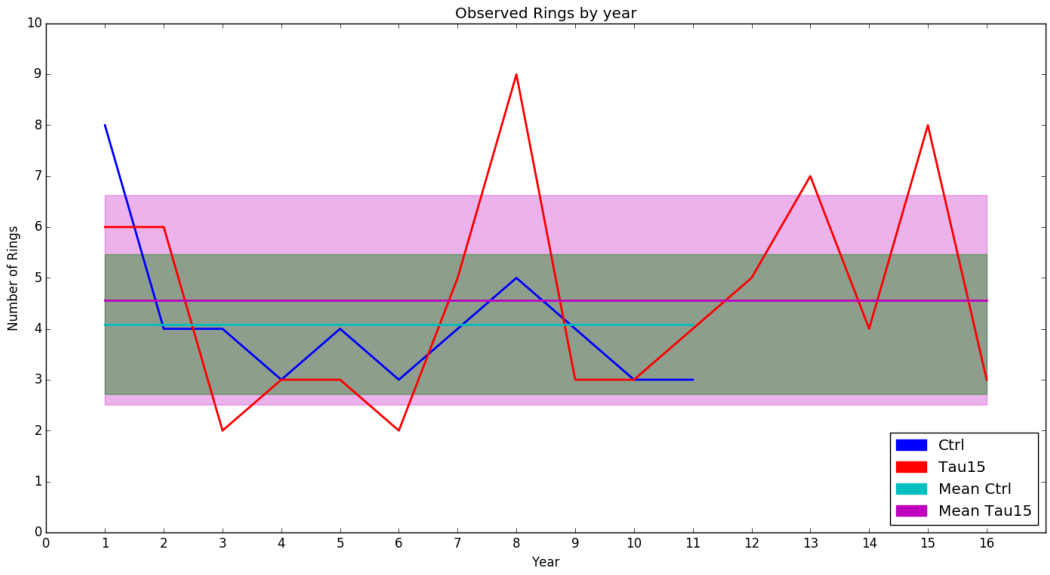

FIGURE 2.14: Agulhas Ring observations by year. (blue) control, (red) tau15, (cyan) mean of control with corresponding one sigma band, (purple) mean of tau15 with corresponding one sigma band.

run by 32%. Why is this? The algorithm was tweaked to check whether the algorithm was to blame for this deficiency. Very little change was found in the number of detected Agulhas Rings indicating that the algorithm is not to blame.

Some of the observed Ring-shedding events of Table 2.1 does not correspond directly to observed Agulhas Rings. The infrared mesurement of Lutjeharms and Ballegooyen, [1988] are strictly retroflection regression events. Infrared measurements in general are short lived, as the Agulhas eddies lose their high surface water temperature quickly. The study by Luthjharms and Cooper, [1996] regarded the less coherent Agulhas filaments. The difference in size between an Agulhas Ring and a mesoscale Agulhas filaments can overlap in the lower radii Agulhas Rings. Agulhas Ring formation is not strictly limited to the retroflection pinch-off events but can also happen via ring mergers west of the retroflection [Wang, Beron-Vera, and Olascoaga, 2016]. Therefore it can be quite difficult to distinguish large filaments from small Agulhas Rings especially with the somewhat sporadic altimeter data used by the authors.

The mean annual ring generation between the control and tau15 data increase by 12%. These 12% are however within one sigma as shown in Figure 2.14. This indicates that increasing wind stress on the southern ocean either has no effect on the mean Agulhas leakage in the form of Agulhas Rings, or the 15% increase in wind stress is too low to see any change outside of the natural variability.

Observations of Agulhas Ring shedding never found any seasonal dependencies as is also witnessed in the control data. A seasonal cycle arises in the tau15 data. Why this is the case, is unknown but as noticed in Figure 1.6 the lack of connection

between upstream and downstream variability could indicate that upstream effects in the tau15 data has less effect on the retroflection giving rise to a seasonal cycle. A seasonal cycle would thus be the norm if not disprupted by upstream effects in the Agulhas Current as is the case in the control data.

TABLE 2.1: Number of Agulhas Ring-shedding events as estimated by different authors

Numbers per year	Author	Device	Time period
9 (6-12)	Lutjeharms and Ballegooyen, [1988]	infrared	1978-1983
5	Gordon and Haxby, [1990]	altimeter	Nov. 1986 to Nov. 1987
6 (4-8)	Feron and Ruijter, [1992]	altimeter	Nov. 1986 to Dec. 1989
7	Ballegooyen, Grundlingh, and Lutjeharms, [1994]	altimeter	Dec. 1986 to Dec. 1988
6	Byrne, Gordon, and Haxby, [1994]	altimeter	Nov. 1986 to Aug. 1989
5 (4-6)	Garzoli et al., [1996]	echo sounder	June. 1992 to Oct. 1993
6.5	Luthjharms and Cooper, [1996]	infrared	1987-1991
5.2 (4-6)	Goni et al., [1997]	altimeter	Sept. 1992 to Dec. 1995
5 (4-6)	Mathijs W. Schouten and Leeuwen, [2000]	altimeter	Nov. 1993 to Dec. 1996
5.5 (5-6)	Souza et al., [2011]	altimeter and floats	Jan. 2005 to Dec. 2008

Mean annual number of Agulhas Rings adapted and expanded from Ruijter et al., [1999]. Annual variability is given within parenthesis when avaiable.

In the next chapter we will investigate one of these upstream effects and proposed trigger mechanisms for Agulhas Ring shedding.

Chapter 3

Natal Pulses

3.1 Background

The Natal Pulse is a cyclonic eddy which has opposite spin of the Agulhas Ring. It suddenly appears as a bulge in the otherwise normal and stable current along the coast of South Africa and moves down the Agulhas Current causing a depression of the SSH. The Natal Pulse is an interesting phenomenon because as it enters the retroflection, is has the power to cause a pinch-off and thereby plays an important role in the shedding of Agulhas Rings.

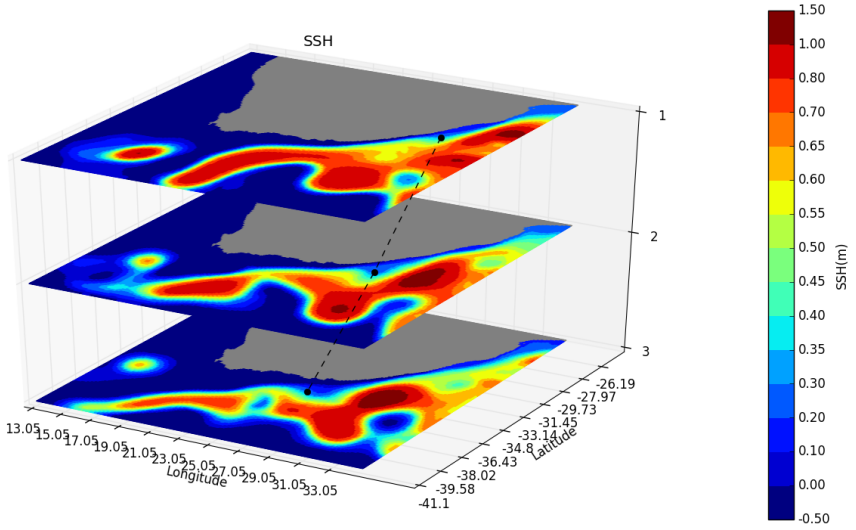

FIGURE 3.1: A Natal Pulse is shown during three consequtive months.

The cyclonic Natal Pulse was first observed in an accidental oil spill off the South African coast [Grundlingh, 1983]. After that event it was unintentionally measured during mapping of the Agulhas Current. Hydrographic sections of the Agulhas Current showed the lateral position of the currents coastal core had a low variability relative to the African continental slope of $15km$. However in the analysis 23% of the 307 sections taken between Port Elizabeth (25°E) (see Figure 3.2 for positional

reference) and Cape St. Lucia(32°E) were discarded due to the current core either being too weak, a pertubation of 100km was measured or lay beyond the 200km range of the station lines [Grundlingh, 1983]. A similar study conducted in the Natal Bight (bay) off the coast of Port Edward(30°E), Durban(31°E) and Richards Bay(32°E) found the deviations of the current to range between 25 and 100km [Pearce, 1977]. Apart from these deviations the Agulhas Current landward core is believed to have little displacement [Lutjeharms and Roberts, 1988]. This is supported in the data by the elongated minima in the variance of Figure 3.2 just off the African coast.

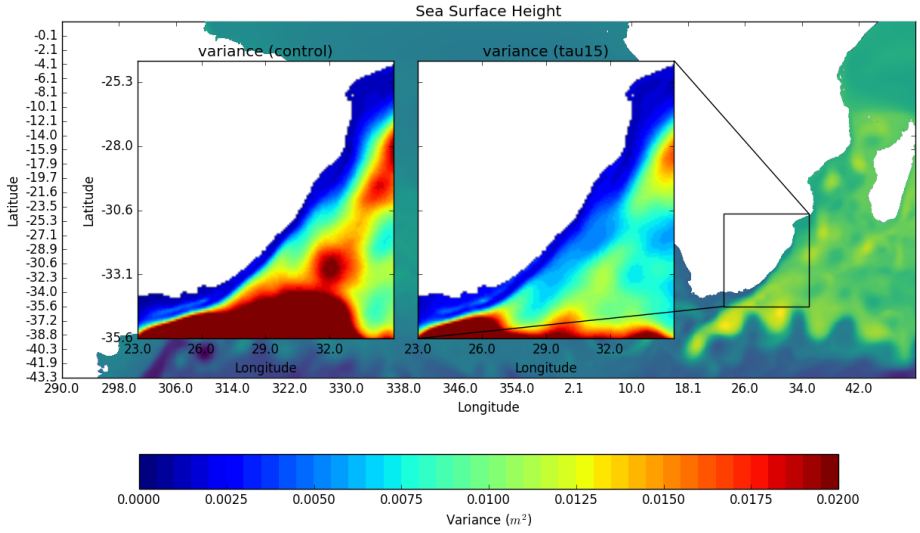

FIGURE 3.2: The temporal variance of the data sets zoomed in on the Natal area. Monthly mean SSH map on the bottom for positional reference. Delagoa Bight is in the top right and the Natal Bight is just below.

These Natal Pulses were found to propagate downstream with a phase speed of about 20 cm/s [Grundlingh, 1979] which slows down to around 5 cm/s at the retroflection [Lutjeharms and Roberts, 1988]. The phenomenom was given the name Natal Pulse for its supposed inception area in the Natal Bight. While this is true [Lutjeharms and Roberts, 1988] pulses have also been observed emanating from the north-east adjacent Delagoa Bight [Lutjeharms and Silva, 1987] but are still referenced under the same name[1].

The topography of the Bight is thought to generate cyclonic eddies. They then travel downstream as Natal Pulses while increasing in lateral size [Ruijter, Leeuwen, and Lutjeharms, 1999]. They are thought to be connected in the shedding of an Agulhas Ring and thereby play a crucial role in the inter-ocean exchange of water between the Indian and South Atlantic Ocean [Leeuwen, Ruijter, and Lutjeharms, 2000].

[1]Probably because the Natal Bight is at the coastal limit of South Africa and the Agulhas Current is mainly studied by South African oceanographers

Many transient phenomenons of the Agulhas Current have been linked to Agulhas Ring formation but mainly through the triggering of Natal Pulses. From observing the data used in this thesis it is clear that Mozambique and Madagascar cyclonic and anti-cyclonic eddies may play a role. Cyclonic eddies from south of the retroflection can be absorbed into the retroflection causing a shortening. Large cyclonic and anti-cyclonic eddies in the Agulhas current itself can also possibly be linked to a pinch off of the retroflection.

In this chapter we will discuss the identification, detection, tracking and analysis of Natal Pulses in order to later see if they act as a trigger mechanism for Agulhas Ring shedding.

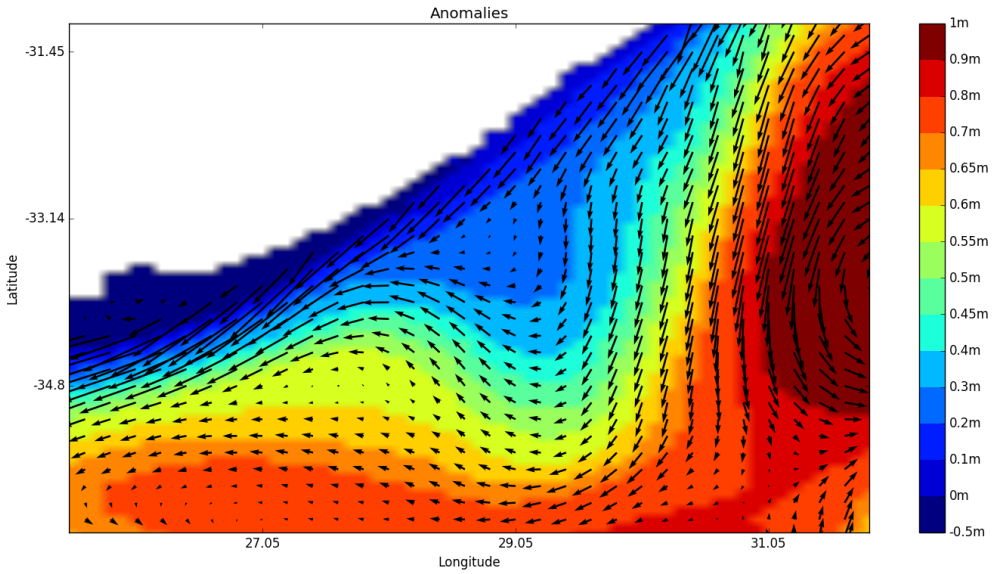

FIGURE 3.3: Geostrophic velocities of a Natal Pulse.

3.2 Identification and definition

There are many transient features in the Agulhas Current. A Natal Pulse is defined as:

1. Spawns at the Natal Bight or further upstream
2. Is cyclonic by nature
3. Current is locally displaced seaward from the continent
4. Travels downstream the Agulhas Currents continentward side

This definition is necessary as other cyclonic structures are observed near and north of the Natal Bight but are not Natal Pulses. Cyclonic cold water eddies from south of the current also invade the Agulhas Current. Therefore simply measuring anomalies

near the Natal Bight or large meanders near the retroflection does not correspond to an observation of a Natal Pulse. Making sure the condititions are met are important for correct identification of Natal Pulses.

With the Delagoa Bight in the upper right and the Agulhas Retroflection in the lower left of Figure 3.4 shows the mean sea surface height of the Agulhas Current. It is clear from the zoomed in area that a steep height gradient marks the position of the Agulhas Current. The current can then be simply thought of as higher than a certain height contour that encompasses it and vice versa.

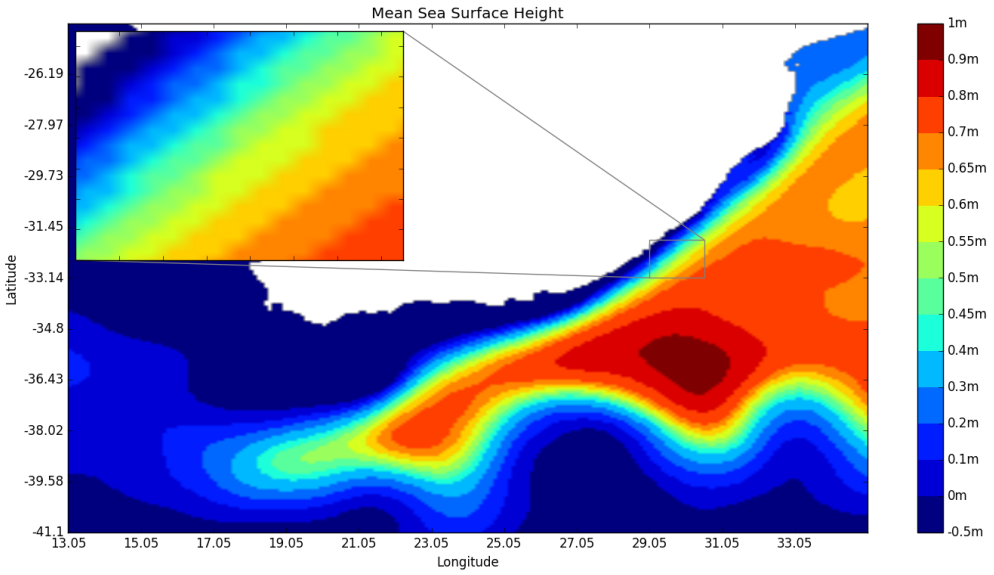

FIGURE 3.4: Mean sea surface height of the Agulhas Current.

The Natal Pulse is visible as a displacement of the Agulhas Current. A good way to describe it, is to follow the displacement the $0.4m$ SSH contour from its median position. This lets us create a 2D displacement map of the contour which is shown by the highlighted areas in Figure 3.5.

A detailed description of the displacement map is as follows: First, all data points with a median below the choosen contour is eliminated. Secondly all data points with a SSH above the contour is eliminated. What remains is a boolean map. The displacement is highligted in Figure 3.5 and a Natal Pulse is revealed. Summation over the size of highlighted area in the displacement map gives the total displaments caused by a Natal Pulse. Zonal and meridional summation of several maps in time as shown in the following Hovmoller diagrams of Figure 3.6 and 3.7 are used to visualize southward and eastward propagation of displacements as connected lines in the diagrams. This is a standard method used to show signal propagation through time.

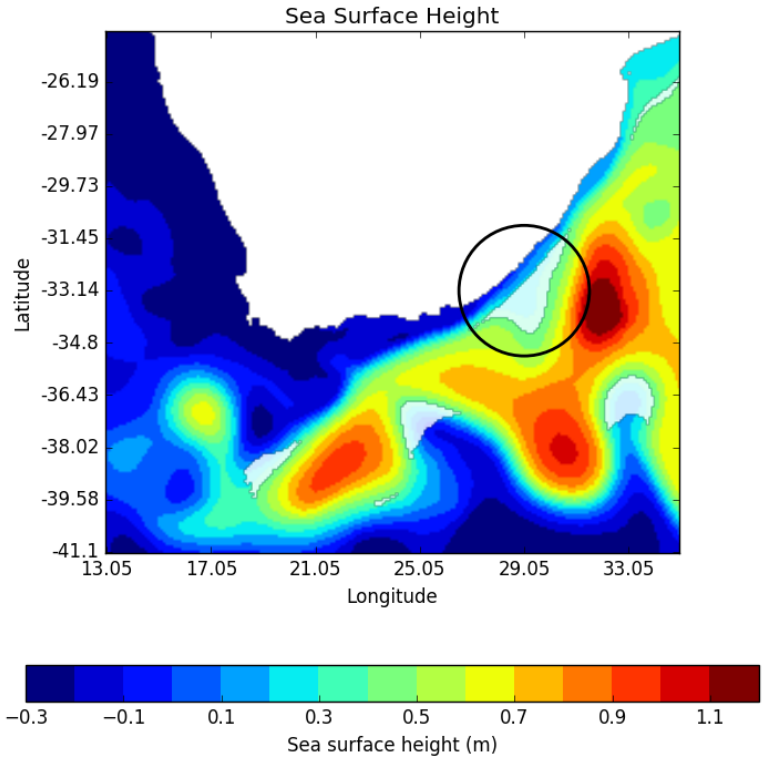

FIGURE 3.5: Displacements of the $0.4m$ SSH contour from the mean is highlighted. One of these is a Natal Pulse (circled).

3.3 Origin of the Natal Pulse

Hovmoller diagrams of the total displacement in zonal and meridional directions are shown in Figure 3.6 and Figure 3.7. The Delagoa Bight coordinates are 36°E, 26°S. While the longitudinal spectrum is filled with noise north the bight the latitudinal reveals slow anomalies propagating southward. Some seems to originate from as far north as 17°S which would place it at the narrowest place between Africa and Madagascar in the Mozambique Straight. By entering this parth of the straight anti-cyclonic Mozambique eddies could generate cyclonic eddies (see Figure 3.8) that propagate downstream near the coast. Alternatively the cyclonic eddies could be caused by general nonlinearities in the flow. This specific part of the Mozambique straight has a significant decrease in variability between the data sets as seen by Figure 1.7 and Figure 1.8. Another interesting disparity between the control and tau15 Hovmoller diagrams is the almost 5 year halt in generation of Natal Pulses between month 20 and month 80 seen in Figure 3.7. This could be related to the severed link in Figure 1.8 between upstream and downstream variance compared to the control in Figure 1.7. Another cause for this could be Madagascar eddies are shed further south and therefore no longer enter the Delagoa Bight area.

It is however clear that most if not all Natal Pulses originate from the Delagoa Bight at about 26°S 36°E or further north.

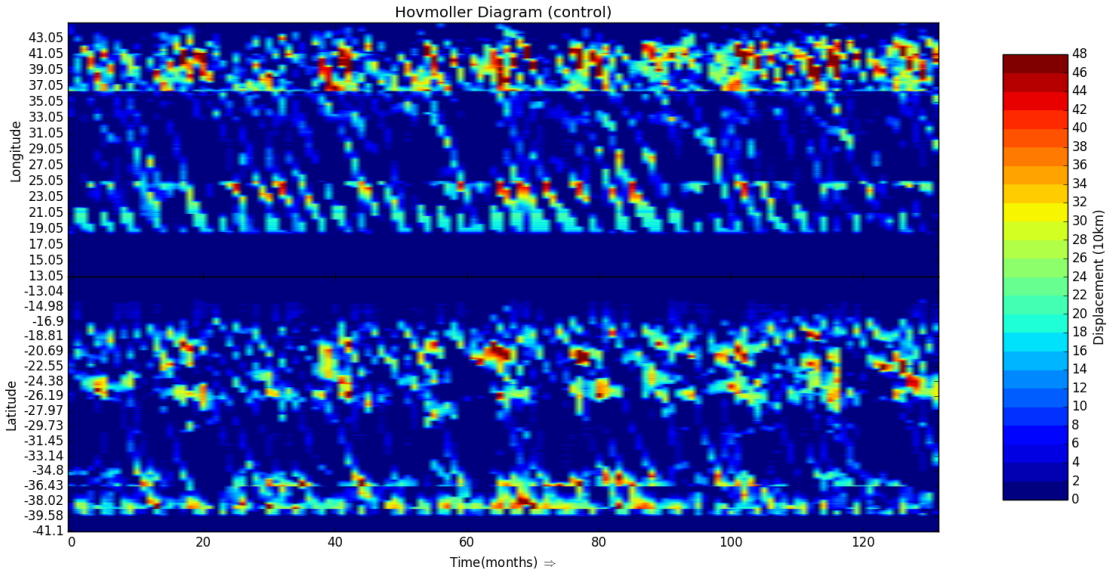

FIGURE 3.6: Hovmoller plot showing displacement propagation of anomaly signal in control data

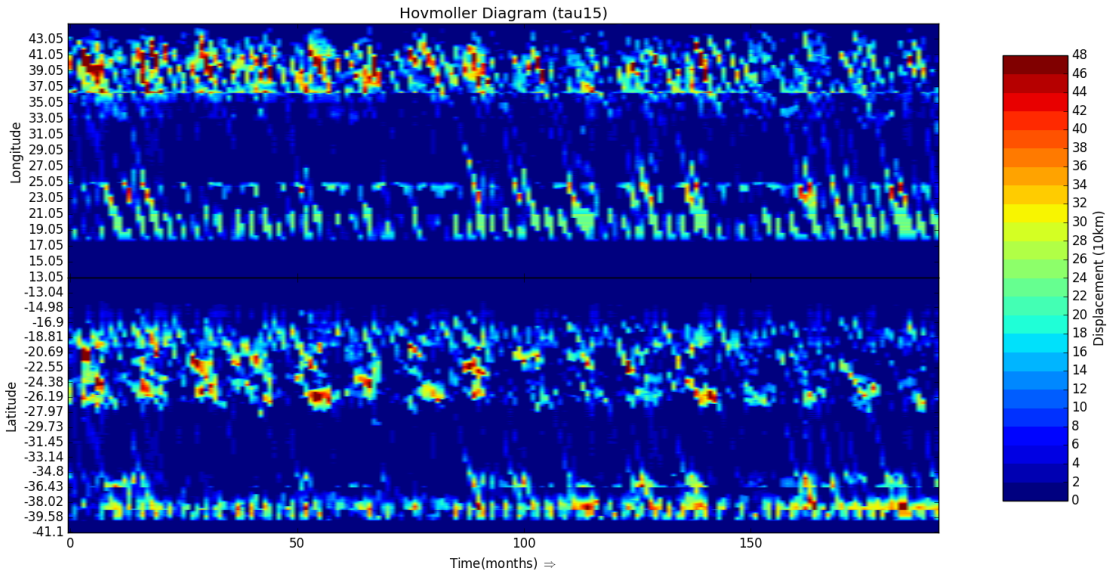

FIGURE 3.7: Hovmoller plot showing displacement propagation of anomaly signal in tau15 data

The southward movement on the western boundary of the Natal Pulse immediatly rules out known atmospheric waves such as Kelvin waves as they would propagate northward here. From the readings of the Hovmoller diagrams and Figure 3.8 cyclonic meanders of about $200km$ in diameter are created near the coast by flow

into the narrowest part of the Mozambique straight possibly by Mozambique eddies as there are no cyclonic eddies entering from the north. Their size however decrease significantly before reaching the Delagoa Bight.

Figure 3.8 also shows cyclonic and anti-cyclonic eddies eminating from Madagascar and moving eastward towards the Delagoa Bight. The conjunctions of eddies meeting at the bight may play a role in Natal Pulse genesis. The Natal Pulse production method is clearly complicated.

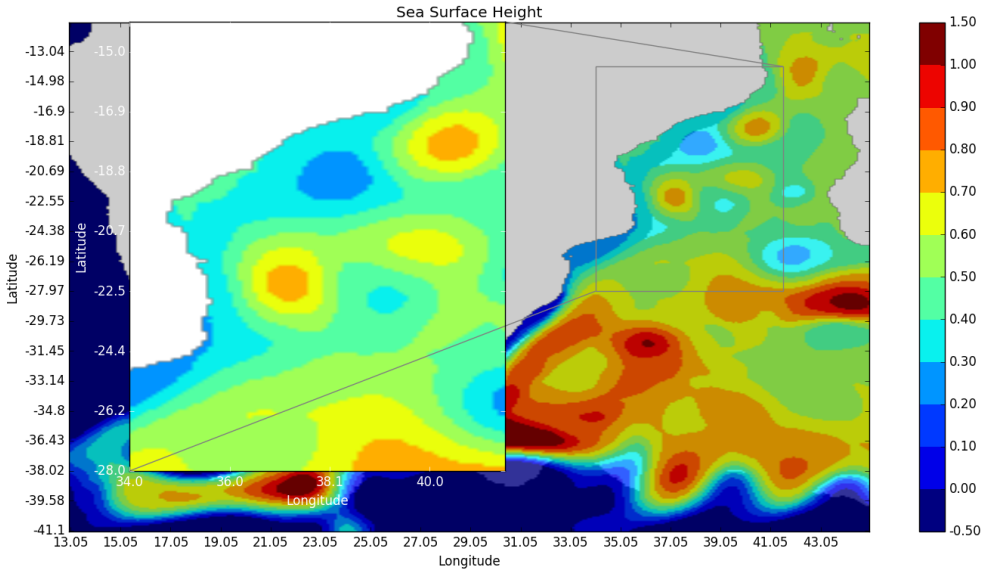

FIGURE 3.8: Eddies of the upper Agulhas Current (control). Two cyclonic at $20.7°S$ and a decayed one at $24.4°S$ just north of the Delagoa Bight are highlighted by the displacement map. Three anti-cyclonic Mozambique eddies in the Mozambique Straight are also visible. Similar eddies is also being emitted from South of Madagascar

3.4 Detection of anomaly interest points

Each displacement anomaly found such as the circled one of Figure Section 3.5 is at first treated as a potential Natal Pulse candidate. In order to describe the anomalies, multiple key points are gathered using a similar method to the one described in Section 2.2[2].

Key points are represented by Scale Invariant Feature Transform (SIFT) descriptors [Lower, 2004], which in short is a histogram of angles between zonal and meridional gradients in an area around the key point[3]. This specific descriptor is used

[2]The hundreds of lines of code making up the algorithm used in this chapter can be optained upon request from the author.

[3]SIFT descriptors were found to be superior for the problem at hand compared to a simple sum of squared differences between key points. An indepth comparison will not be provided.

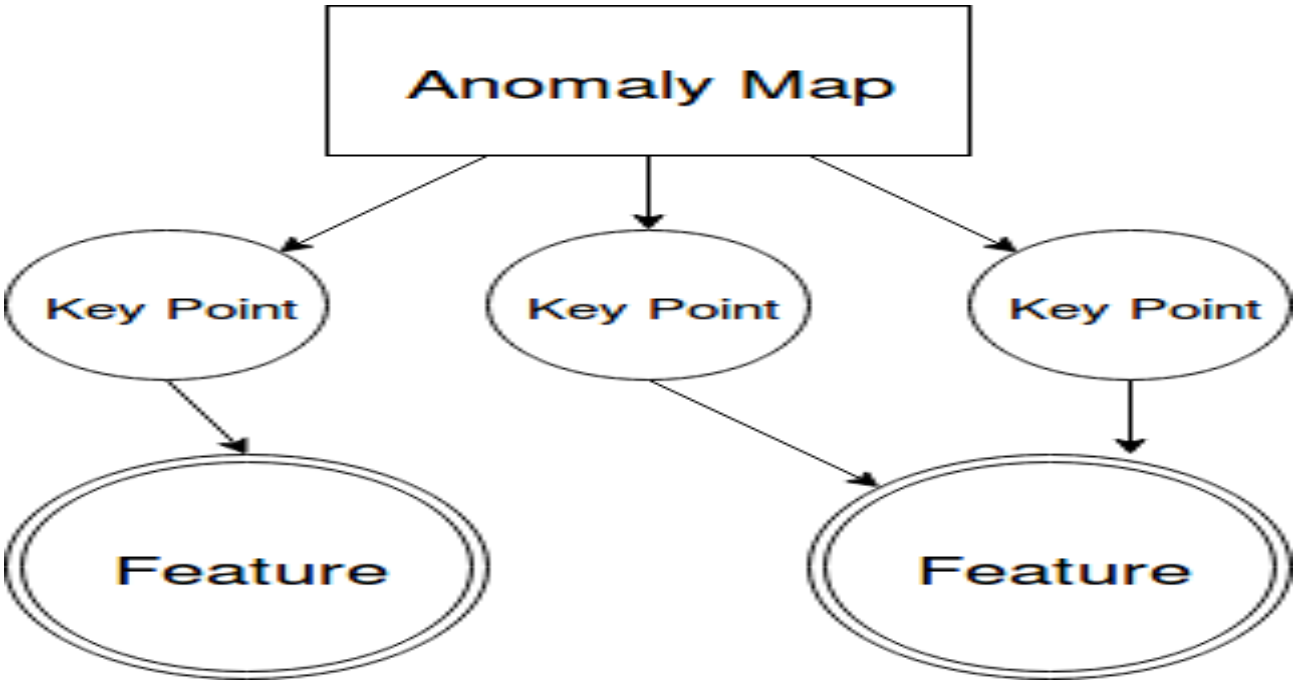

FIGURE 3.9: Key points are detected from the anomaly map then assigned to their local feature.

because the African continent (and thereby the Agulhas Current) always provide almost exactly the same angle and the gradient angle are the approximated direction of geostrophic flow between the Natal Bight and the retroflection.

The key points that are close to eachother describes the same feature(anomalies). Hence a feature is made up by the several local key points that in turn each have individual descriptors.

Features on the south side of the current are not in correspondance can easily be filtered out by looking at the dominant angles between gradients.

3.5 Tracking

Features found in one frame are matched to features in the next by minimizing the sum of squared differences between key points SIFT descriptors. Intuitively one can say a feature lets each key point within cast a vote and the feature with the most votes is the best match (see Figure 3.10).

Once two features has been succesfully matched, they form a track through time. Figure 3.1 shows three months of a six months long track, while Figure 3.11 shows all Natal Pulse tracks found with the algorithm which are in accordance with what one would expect from the known paths of Natal Pulses.

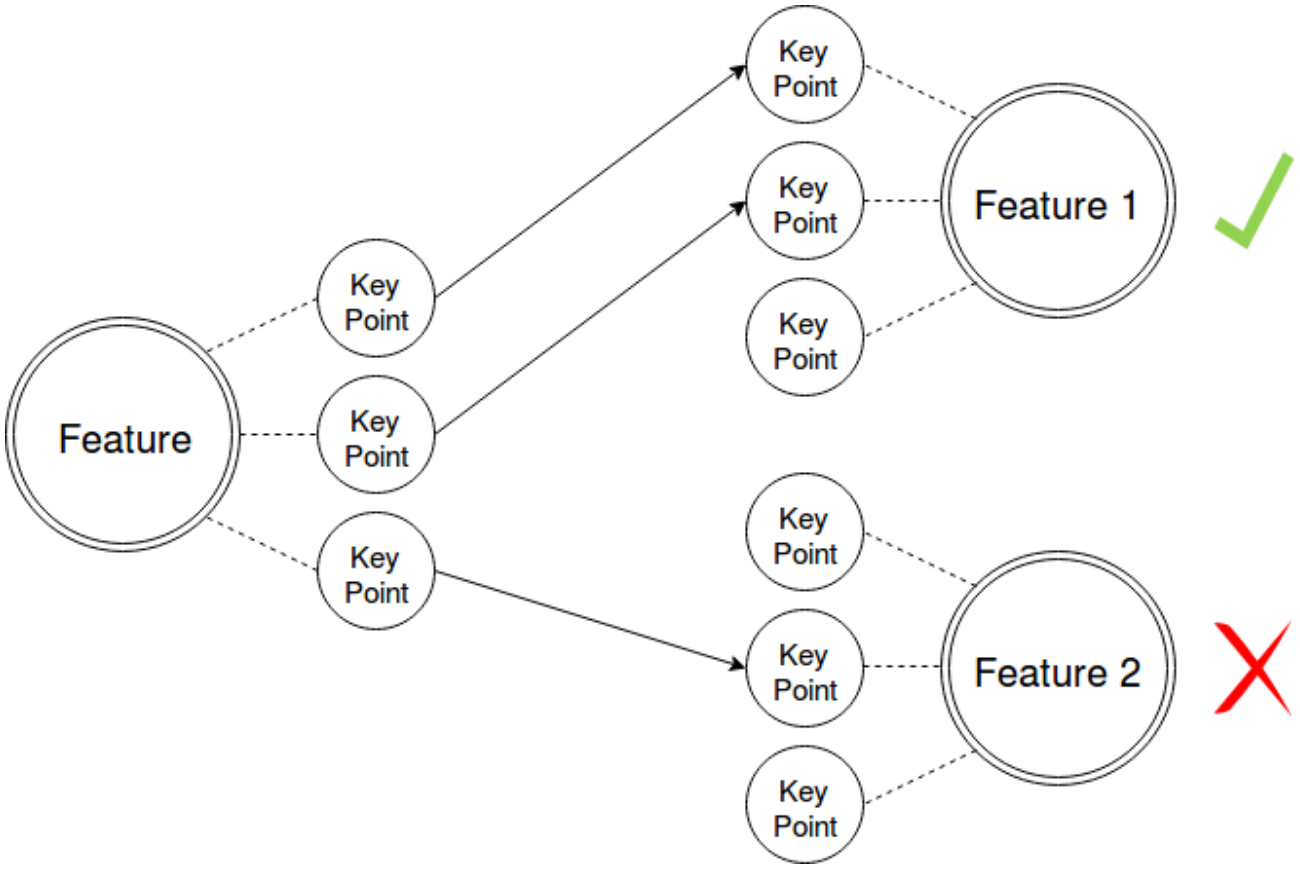

FIGURE 3.10: Simple flow chart explaining the tracking algorithm. Left Feature is found at time $t = i$ and right at $t = i + 1$. Two key points belonging to the left feature matches with the key points of Feature 1 while only one is matched with a key point of Feature 2. Feature 1 is then considered the best match for the Feature.

3.6 Velocity of Natal Pulses

The velocity of the Natal Pulse as it moves downstream can be found from Natal Pulse tracks shown in Figure 3.11. The mean velocity is shown in Figure 3.12. The Natal Pulse has a translational speed of 11-13cm/s as it enters the Natal Bight speeding up to 13-15cm/s below the bight and later slows down to 8-11cm/s and finally stops at the retroflection or speed up as a pinch-off. These mean velocities have variation those given by Grundlingh, [1979] and Lutjeharms and Roberts, 1988.

3.7 Is the Natal Pulse a trigger mechanism for Agulhas Rings?

The Agulhas Current retroflection has a natural cycle. First it lengthens and then subsequently closes in on itself causing a pinch-off of the current. Hereby, the western position of the retroflection regresses eastward (referred to as *regression*).

Figure 3.13 and Figure 3.14 combines Agulhas Ring detection with the Natal

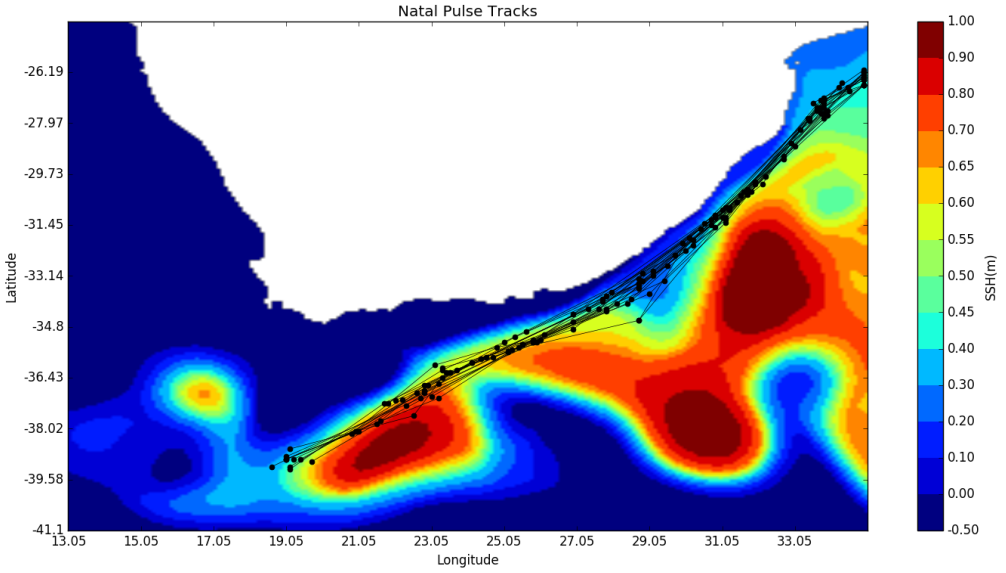

FIGURE 3.11: Natal Pulse tracks found from the algorithm explained in this chapter.

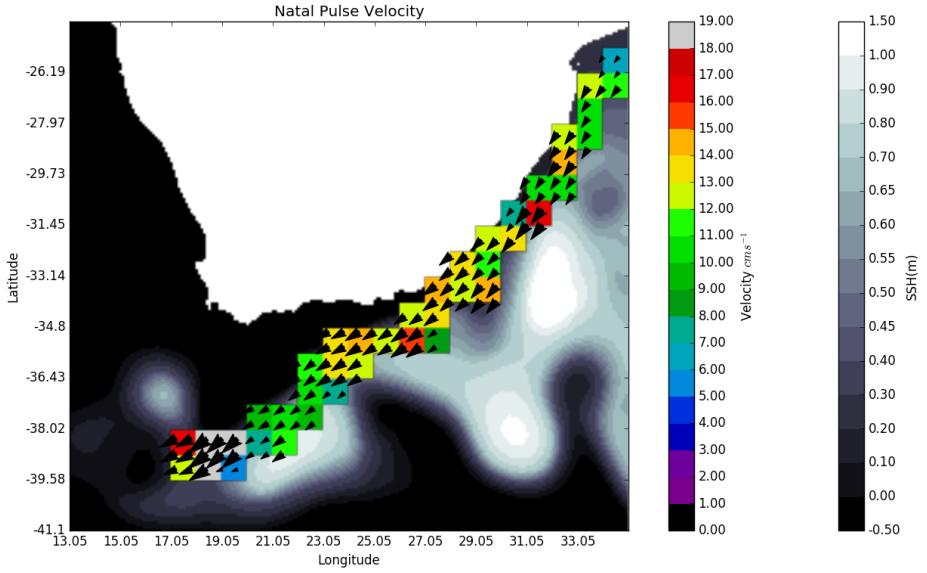

FIGURE 3.12: Mean translational velocity of the Natal Pulse as is propagates downstream

Pulse to seek a clear picture of the correlation between the two. The natural lengthening/regression cycle of the retroflection is captured in the diagrams. A displacement of about 200km is needed for this (as can be seen from Figure 1.3 and Figure 1.4). There are two type of regression events visible in the Hovmoller diagrams. A large shortening of the retroflection at 25°E and a small at 21°E. More often than not the large events are preceeded by a Natal Pulse. The Natal Pulse thus amplifies the regression of the retroflection.

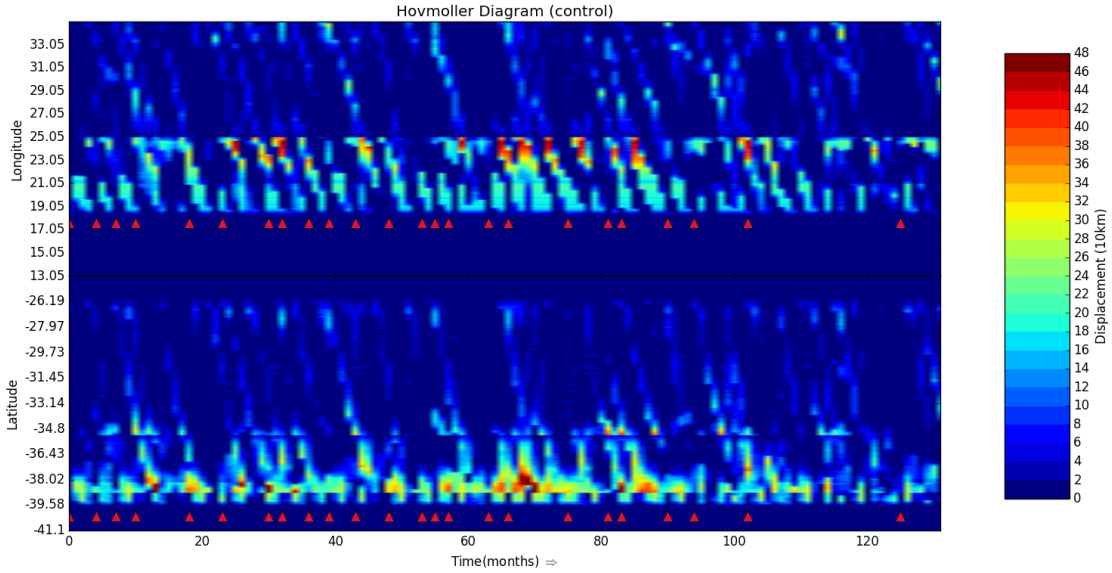

FIGURE 3.13: Correlation between Natal Pulses and Agulhas Ring detections near the retroflection. Crimson triangles denotes detection of an Agulhas Ring within $500km$ of the retroflection

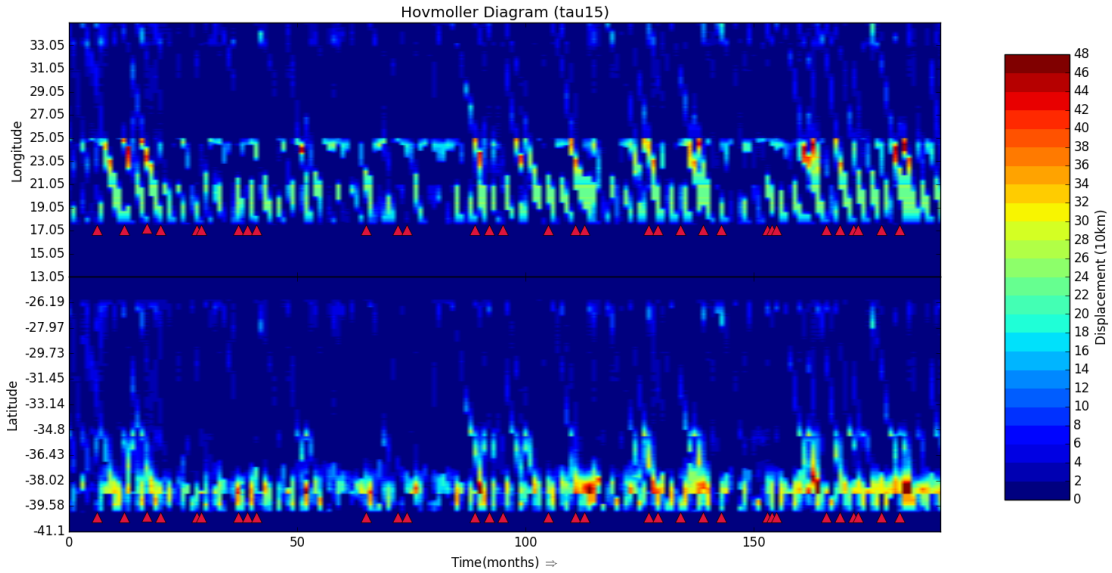

FIGURE 3.14: Correlation between Natal Pulses and Agulhas Ring detections near the retroflection. Crimson triangles denotes detection of an Agulhas Ring within $500km$ of the retroflection

Agulhas Ring detections near the retroflection (red triangles) are preceeded by a shortening of the Agulhas Current. It is obvious that pinch-offs and thereby regressions of the Agulhas Current retroflection are needed for the formation of Agulhas Rings. The Natal Pulse can induce such a regression and thereby create the right conditions for Agulhas Ring formation. In Table 3.1 the Hovmoller diagrams latitude

and longitude spectrums are used in combination with the Agulhas Ring algorithm to investigate a direct cause and effect between the two phenomenoms.

The first two entrances of Table 3.1 makes it evident that the number Agulhas Rings and the number of Agulhas Current retroflection regressions are not the same. However there is a similar ratio between the numbers of 0.76 and 0.72 for the control and tau15 data respectively. This indicates that about 30% of the rings are formed by different mechanics than a direct pinch-off. This ratio actually agrees with Lutjeharms and Ballegooyen, [1988] average of 9 regressions per year, however, noting that only 6 Agulhas Rings are shed on average optained from Table 2.1. This would give a ratio of about 2/3. The statistical fluctuations of the 9 regressions are however relatively large.

One must also be careful interpreting the other numbers of Table 3.1 since not all the Agulhas Rings where identified (or formed) within the first 500km of the retroflection but at a later time.

A total of 23 Natal Pulses were found in the control data and 19 in the tau15. Respectively 13 and 19 of these preluded an identification of an Agulhas Ring within 500km of the retroflection. In the case of non-Natal Pulse induced regressions there were 11 in the control and 41 in the tau15 data. Of these 9 and 17 Agulhas Rings were found near the retroflection in the control and tau15 data respectively. The number of Agulhas Rings detected close to the retroflection is unfortunately too low to reliably determine the effect of Natal Pulses on Agulhas Ring formation by the information presented in Table 3.1 simply due to statistical fluctuations.

TABLE 3.1: Effect of Natal Pulse on Agulhas Ring formation

	Control	Tau15
Total number of observed Agulhas Rings	45	73
Total number of Agulhas Current retroflection regressions	34 $\pm$1	53
Total number of Agulhas Rings observed near retroflection	24	32
Total number of regression following a Natal Pulses	23	19$\pm$1
Agulhas Rings observed after Natal Pulse	13	12$\pm$1
Agulhas Rings observed after Agulhas Current regression[4]	9$\pm$1	17$\pm$2

Estimated Natal Pulse effect on Agulhas Ring formation. Numbers in this table are estimated from Figure 3.13 and Figure 3.14. Agulhas Rings near the retroflection are within 500km of its eastern point.

Chapter 4

Summary an conclusion

The Agulhas leakage in the form of large anti-cyclonic eddies, known as Agulhas Rings, were explored in a high resolution $1/10^{\circ}$ general circulation model. Two model runs were investigated using monthly mean sea surface height data; a control run and a perturbation run (tau15) with 15% increase in wind stress on the southern ocean. An algorithm was developed specificaly to detect Agulhas Rings. Aditionally a proposed trigger mechanism for Agulhas Ring-shedding, the Natal Pulse, was investigated.

A total of 45 rings were found during the 11 years of control data and 73 in the 16 years of tau15. Mean annual Agulhas Ring production are within statiscal fluctuations of each other and can therefore be considered the same. Wind stress on the Southern Ocean either has no say in Agulhas leakage via Agulhas Rings, or the 15% increase is too low and within natural variability.

The dynamics of the Agulhas Rings between the data were the same and match estimates from studies using remote sensing measurements. However a 14.5% increase in translational velocity from $5.4 \pm 0.6cm/s$ in the control to $6.2 \pm 0.8cm/s$ of the tau15 data was found. A mean radius of $140km$ was found. The sea surface height of the Agulhas Rings was the same and decreasing in a similar way as those found by Byrne, Gordon, and Haxby, [1994]. Potential vorticity of the Agulhas Rings are constant up to $1000km$ from the retroflection, possibly due to slow acting friction and absorption of smaller anti-cyclonic filaments and eddies, in order to compensate for the increase in planetary vorticity (decrease in Coriolis foce). After this point the potential vorticity of Agulhas Rings slowly dissipates during their 4000-5000km journey across the Atlantic Ocean.

A seasonal cycle is visible in the tau15 data but not in the case for the control. What gives rise to this is unknown but might be due to more water is recirculated in the lower part of the subtropical Indian Ocean gyre instead of. This in turn could lead to the lower variability observed in the Mozambique straight, south of Madagascar and the upper part of the Agulhas Current.

The tau15 data has a four year low in Agulhas Ring generation coinciding with a lack of Natal Pulses. This indicates that the Natal Pulse is a trigger mechanism for Agulhas Ring shedding or an indicator for other upstream phenomenoms that are trigger mechanisms for Agulhas Rings shedding. The Natal Pulses may, however,

cause a large regression of the Agulhas Current retroflection caused by a pinch-off which in turn can lead to an Agulhas Ring shedding event. The number of retroflection regressions are strongly correlated to the total number of Agulhas Rings detected in both data sets. About 70% of Agulhas Ring formations can be explained via this simple relation.

Bibliography

Ballegooyen, R. C. van, M. L. Grundlingh, and J. R. E. Lutjeharms (1994). "Eddy fluxe s of heat and salt from the southwest Indian Ocean into the southeast Atlantic Ocean: A case study". In: *Journal of Geophysical Research* 99.

Biastoch, A. et al. (2009). "Increase in Agulhas leakage due to poleward shift of Southern Hemisphere westerlies". In: *Nature* 462.

Byrne, Deirdre A., Arnold L. Gordon, and William F. Haxby (1994). "Agulhas Eddies: A Synoptic View Using Geosat ERM Data". In: *Journal of Physical Oceanography* 25.

Feron, R. C. V. and W. P. M. De Ruijter (1992). "Ring Shedding in the Agulhas Current System". In: *Journal of Geophysical Research* 97.

Garzoli, S. L. et al. (1996). "Variability and sources of the southeastern Atlantic circulation". In: *Journal of Marine Research* 54.

Goni, G. J. et al. (1997). "Agulhas ring dynamics from TOPEX/POSEIDON satellite altimeter data". In: *Journal of Marine Research* 55.

Gordon, Arnold L. and William F. Haxby (1990). "Agulhas Eddies Invade the South Atlantic: Evidence From Geosat Altimeter and Shipboard Conductivity-Temperature-Depth Survey". In: *Journal of Geophysical Research* 95.

Grundlingh, M. L. (1979). "Observation of a Large Meander in the Agulhas Current". In: *Journal of Geophysical Research* 84.

— (1983). "On the course of the Agulhas Current". In: *South African Geographical Journal* 65.

Houry, Sabine et al. (1987). "Brunt-Vaisala Frequency and Rossby Radii in the South Atlantic". In: *Journal of Physical Oceanography* 17.

Jochum, M. and Carsten Eden (2015). "The Connection between Southern Ocean Winds, the Atlantic Meridional Overturning Circulation, and Indo-Pacific Upwelling". In: *Journal of Climate* 28.

Kalnay, Eugenia (2003). *Atmospheric Modeling, Data Assimilation and Predictability*. Cambride Universite Press.

Leeuwen, P. J., W. P. M. de Ruijter, and J. R. E. Lutjeharms (2000). "Natal pulses and the formation of Agulhas rings". In: *Journal of Geophysical Research* 105.

Lower, David G. (2004). "Distinctive Image Features from Scale-Invariant Keypoints". In: *International Journal of Computer Vision* 60, pp. 91–110.

Luthjharms, J. R. E. and J. Cooper (1996). "Interbasin leakage through Agulhas current filaments". In: *Deep-Sea Research* 43.

Lutjeharms, J. R. E. and R. C. Van Ballegooyen (1988). "The Retroflection of the Agulhas Current". In: *Journal of Physical Oceanography* 18.

Lutjeharms, J. R. E. and H. R. Roberts (1988). "The Natal Pulse: An Extreme Transient on the Agulhas Current". In: *Journal of Geophysical Research* 93.

Lutjeharms, J. R. E. and A. Jorge da Silva (1987). "The Delagoa Bight eddy". In: *Deep-Sea Research* 35.

Mathijs W. Schouten, Will P. M. de Ruijter and Peter Jan van Leeuwen (2000). "Translation, decay and splitting of Agulhas rings in the southeastern Atlantic Ocean". In: *Journal of Geophysical Research* 105, pp. 21,913–21,925.

Olson, Donald B. and Robert H. Evans (1985). "Rings of the Agulhas Current". In: *Deep-Sea Research* 33.

Pearce, A. F. (1977). "Some features of the upper 500m of the Agulhas Current". In: *Journal of marine research* 35.

Pedlosky, Joseph (1996). *Ocean Circulation Theory*. Springer.

Pichevin, Thierry, Doron Nof, and Johann Lutjeharms (1998). "Why Are There Agulhas Rings?" In: *Journal of Physical Oceanography* 29.

Ruijter, W. P. M. de, P. J. Leeuwen, and J. R. E. Lutjeharms (1999). "Generation and Evolution of Natal Pulses: Solitary Meanders in the Agulhas Current". In: *Journal of Physical Oceanography* 29.

Ruijter, W. P. M. de et al. (1999). "Indian-Atlantic interocean exchange: Dynamics, estimation and impact". In: *Journal of Geophysical Research* 104.

Sebille, E. van et al. (2009). "A weaker Agulhas Current leads to more Agulhas leakage". In: *Geophysical Research Letters* 36.

Small, R. Justin et al. (2014). "A new synoptic scale resolving global climate simulation using the Community Earth System Model". In: *Journal of Advances in Modeling Earth Systems* 6, pp. 1065–1094.

Souza, J. M. A. C. et al. (2011). "Estimation of the Agulhas ring impace on meridional heat fluxes and transport using ARGO floats and satellite data". In: *Geophysical Research Letters* 38.

Wang, Y., F.J. Beron-Vera, and M.J. Olascoaga (2016). "The life cycle of a coherent Lagrangian Agulhas Ring". In: *Journal of Geophysical Research* 10.